UNIVERSITÀ DEGLI STUDI DI PADOVA

DIPARTIMENTO DI INGEGNERIA CIVILE, EDILE E AMBIENTALE

Department of Civil, Environmental and Architectural Engineering

Tesi di laurea magistrale

Mapping heatwaves and climate extremes in the geopolitical region of Kurdistan

Supervisor: prof. Salvatore Pappalardo
Author: Sima Ghahremani Dehbokri

Academic year: 2024-2025

Abstract

Heatwaves and extreme surface temperatures are intensifying in many geographical areas of the world due to climate change, posing critical risks to urban populations, ecosystems, and infrastructure. However, the impacts of such extremes in politically fragmented and underrepresented areas such as Kurdistan are still poorly studied. This thesis addresses this knowledge gap by analyzing the spatial distribution of heatwave events and Land Surface Temperature (LST) anomalies across four cities in the Kurdistan region Erbil, Diyarbakır, Kobani, and Urmia—located in Iraq, Turkey, Syria, and Iran, respectively. The study aims to quantify localized heat hazard, identify UHI effects, and examine how land cover types influence thermal patterns under extreme climatic conditions. To achieve this, a multi-source geospatial approach was applied, combining historical climate records from ERA5 and CMIP6, satellite-derived LST from Landsat 8 and 9, and high-resolution land cover data from ESA WorldCover 10 m. QGIS software was used to analyze spatial relationships between surface heat intensity, land use composition, and urban morphology within both municipal boundaries and 20 km peri-urban buffers. The results show that extreme UHI effects occurred in Erbil and Diyarbakr, where dense urban development and low vegetation resulted in LST values exceeding 60 °C of LST. In contrast, Kobani and Urmia revealed thermal hotspots in ecologically degraded or abandoned zones rather than in their urban cores. These findings highlight the role of vegetation loss, land abandonment, and urban form in shaping localized heat vulnerability. By providing a replicable methodology for spatial heat risk assessment, this research contributes new insights into climate resilience planning in complex geopolitical contexts. The results emphasize the need for integrated land use strategies and green infrastructure to mitigate the escalating impacts of extreme heat in the Kurdistan region and similar data-scarce environments.

Keywords: Urban Heat Islands, Climate Change, LST, Land Cover, Kurdistan, Landsat-8 and 9, QGIS

For Matt and all of those who are prepared to fight for freedom.

Contents

1 Introduction **1**

1.1 Heat Waves and Climate Change 1

1.1.1 Climate extremes 2

1.1.2 Urban Heat Island 3

1.2 Defining the Kurdistan geopolitical region 4

1.2.1 Historical Background of the Kurds 5

1.2.2 Where is Kurdistan 5

1.2.3 Demographic Profile of Kurdistan 7

1.2.4 Why Kurdistan 8

1.3 General Aim 9

1.3.1 Specific Aims 9

2 Data and Methods **13**

2.1 Data Collection 13

2.1.1 Study Cases in Kurdistan 13

2.1.2 Land Cover Data 15

2.1.3 Climate Data (CMIP6 and ERA5) 17

2.1.4 Climate Data Selection and Configuration 17

2.1.5 Land Surface Temperature and Urban Heat Island calculation 19
2.1.6 QGIS and Satellite Imagery (Earth Explorer) 20
2.2 GIScience Approach 21
2.3 Data Analysis 21
2.3.1 Climate extreme calculation in Python 23
2.3.2 Hot Day Frequency and Duration 23
2.3.3 LST–Land Cover Relationship 24

3 Results and Discussion **27**

3.1 Climatic analysis and identification of hotdays 27
3.2 Urban Heat Island analyses 33
3.3 Land Cover Composition 47
3.4 Land use and land cover analyses 48
3.4.1 Diyarbakir 48
3.4.2 Erbil 50
3.4.3 Kobani 52
3.4.4 Urmia 54

4 Conclusions **59**

Bibliography **60**

Sitography **67**

1 Introduction

1.1 Heat Waves and Climate Change

Across the globe, hot days are getting hotter and more frequent, while we are experiencing fewer cold days(c2es heatwaves).Hot extremes (including heatwaves) have become more frequent and more intense across most land regions since the 1950s (IPCC, 2021). This increase is a direct result of anthropogenic greenhouse gas emissions, which have raised the Earth's global average surface temperature by approximately 1.1 ° C since preindustrial times (IPCC, 2021). The Mediterranean, Middle East, and semi-arid regions are identified as climate change hotspots where heatwave intensity and duration are accelerating. Heatwaves in 2023 contributed to tens of thousands of excess deaths and large-scale crop failures across Europe, North Africa, and Asia (WMO, 2023). These events illustrate the compounding socio-environmental consequences of extreme heat on human health, agricultural productivity, water availability, and infrastructure stability. Drought also affects the vegetative state by reducing the photosynthetic activity of plants (Yang et al., 2021), leading to a decline in crop productivity. Moreover, when vegetation is stressed they shift from beeing carbon sink to carbon source. Abandoned and sparsely vegetated lands exhibit significantly higher surface temperatures than adjacent vegetated areas during heatwaves, creating thermal feedback loops that further increase local heating (Liu et al., 2023). This phenomenon intensifies particularly in peri-urban and degraded rural zones, where ecological deterioration and lack of shading amplify surface heat. Urbanization has intensified local warming, especially during nighttime, and this trend is expected to continue unless green infrastructure is systematically implemented (IPCC, 2021). These findings underscore the urgent need to address heatwave vulnerability through integrated climate action, ecological restoration, and adaptive urban planning. As climate extremes escalate in frequency and magnitude, understanding their dynamics is essential for protecting vulnerable populations and building resilient infrastructure systems in Kurdistan and similar regions.

1.1.1 Climate extremes

Some of the most severe effects of global warming will be related to an increase in the frequency and intensity of extreme events. The regional maximum temperature on land is expected to increase more than the mean global temperature. Together with greater temperature variability, this will result in more intense and longer heatwaves. Heat waves can greatly reduce labor productivity and affect human health, with a documented relationship existing between extreme heat events and increased mortality. (Dosio et al., 2018)Extreme heat can increase the risk of other types of disasters. Heat can exacerbate drought, and hot, dry conditions can in turn create wildfire conditions. Buildings, roads, and infrastructure absorb heat, leading to temperatures that can be 1 to 7 degrees F hotter in urban areas than outlying areas – a phenomenon known as the urban heat island effect. This impact is most intense during the day, but the slow release of heat from the infrastructure (or an atmospheric heat island) overnight can keep cities much hotter than surrounding areas. Rising temperatures across the country pose a threat to people, ecosystems, and the economy.Warmer temperatures enhance evaporation, which reduces surface water and dries out soils and vegetation. This makes periods with low precipitation drier than they would be in cooler conditions.(C2ES2025) Climate change is also altering the timing of water availability. Warmer winter temperatures are causing less precipitation to fall as snow in the Northern Hemisphere, including in key regions like the Sierra Nevada of California. Decreased snowpack can be a problem, even if the total annual precipitation remains the same. This is because many water management systems rely on spring snowpack melt . Likewise, certain ecosystems also depend on snowmelt, which supplies cold water for species like salmon. Because snow acts as a reflective surface, decreasing snow area also increases surface temperatures, further exacerbating drought. Some climate models find that warming increases precipitation variability, meaning there will be more periods of both extreme precipitation and drought. This creates the need for expanded water storage during drought years and increased risk of flooding and dam failure during periods of extreme precipitation. Climate change is making certain regions drier For example, the Southwestern United States has already seen a decrease in annual precipitation since the beginning of the 20th century, and that trend is expected to continue. Estimates of future changes in seasonal or annual precipitation in a particular location are less certain than estimates of future warming, and are active areas of research. However, at the global scale, scientists are confident that relatively wet places, such as the tropics and higher latitudes, will get wetter, while relatively dry places in the subtropics (where most of the world's deserts are located) will become drier. In some areas, droughts can persist through a vicious cycle, in which very dry soils and diminished plant cover absorb more solar radiation and heat up, encouraging the formation of high pressure systems that further suppress rainfall, leading an already dry area to become even drier(C2ES2025a). The Kurdistan region is experiencing unprecedented drought and heat-driven agricultural stress,

with government officials warning of 'crop failure and rising food prices' amid declining water availability (Rudaw, 2025). Dryness, one of the most significant natural hazards, has numerous adverse effects on human activity (Mohammad et al., 2025).

1.1.2 Urban Heat Island

The UHI effect refers to the phenomenon in which urban areas exhibit higher surface and air temperatures than their rural surroundings. There is a clear relationship between the intensity of the urban heat island and the size of the city (Oke (1973). The urban heat island (UHI) effect arises from the transformation of natural landscapes into urban environments, and is primarily driven by the reduction in vegetation and evapotranspiration, the dominance of dark, impermeable surfaces with low albedo, and increased anthropogenic heat emissions (Stone et al., 2010). As a result, the thermal behavior of an urban area is heavily influenced by its surface composition, which has direct implications for selecting effective UHI mitigation strategies. Akbari and Rose (2008) found that the average urban surface composition in four major U.S. metropolitan areas included 29–41% vegetation, 19–25% roofs, and 29–39% paved surfaces. This indicates that over 60% of the urban landscape may consist of hard, man-made materials that are highly absorbent of solar radiation. This temperature increase is directly correlated to the size of the city centre, the main building types (Naumann Formetta, 2020), the salient features intended as urban materials, the greenery, the urban morphology such as the presence of urban canyons, the population density (Sangiorgio et al., 2020), the geography of the city location and topographical features, presence of water bodies, properties of soils (Oke, 1982), climatic conditions and seasonal variations (Mohajerani et al., 2017). All possible combinations of these parameters can create different conditions that may be beneficial or detrimental to city dwellers. In most cases, densely populated urban areas are significantly warmer than surrounding non- urbanised areas. In contrast, a study of some cities in the United States showed that cities built in arid or desert-like environments may experience lower temperatures than surrounding areas, as the urban cores are greener than their surroundings (Bounoua et al., 2015). The thermal difference between urban and rural areas is mainly studied through satellite remote sensing. Many authors have documented the use of satellite remote sensing for the purpose of assessing surface temperature (LST) and UHI spatial and temporal variability mitigation (Liu Zhang, 2005), while other scholars have evaluated the relationship between different vegetation indices and LST (Kumar Shekhar, 2015) or between different land uses and LST (Kumar Shekhar, 2015). In the context of the Kurdistan Region, where rapid urban expansion often lacks coordinated green infrastructure development, cities like Erbil and Diyarbakir are increasingly exposed to intensified UHI effects. Mapping and understanding these spatial patterns is essential for guiding climate-resilient urban development and identifying vulnerable areas requiring targeted interventions.

1.2 Defining the Kurdistan geopolitical region

Figure 1.1: Map of Kurdistan from 1946, published by Elias Modern Press in Cairo

This 1946 map of Kurdistan was published by Elias Modern Press in Cairo by elements of the Kurdish diaspora in Egypt. According to Maria T. O'Shea (2004), the map was 'the first Kurdish projection of all of Kurdistan to be aimed at the outside world' and 'unique in that it had an accompanying text to justify the positions taken' (p. 153). According to the French legend of the map, "The ethniques frontières of Kurdistan are indicated by a zone of hachures d'autant plus mince que the delimitation is more nette. Les autres zones hachurées indicate la position et l'étendue approximative des groupements isolés.' The English pamphlet accompanying the map explains that 'Areas marked by hatchings are those about which information is indefinite.'

This use of visual uncertainty contrasts with later interpretations, where these zones were sometimes used as firm ethnic claims. The inclusion of coastal areas linking the Persian Gulf aligns with other post-WWII maps produced for diplomatic purposes during 1945–1946, emphasizing strategic aspirations for a potential Kurdish state.

1.2.1 Historical Background of the Kurds

Kurds are native inhabitants of their land, and as such, there are no strict beginnings for Kurdish history and origins (Izady,2004.). In modern times, Kurds as an ethnic group are the product of thousands of years of cultural and tribal evolution, descending from ancient groups such as the Guti, Kurti, Mede, Mard, Carduchi, Gordyene, Adiabene, Zila, and Khaldi (Izady, 2004.). Their history also reflects the migration of Indo-European tribes into the Zagros mountain region around 4,000 years ago (KHRP, 1995, p. 6). Similarly to the Highland Scots, the Kurds have a deeply rooted clan-based social structure, historically encompassing over 800 tribes across the region (Saeedpour, 1999). By the seventh century AD, during the Arab conquest of Mesopotamia, the term 'Kurd' was already used to describe these nomadic peoples. The word 'Kurdistan', meaning 'the land of Kurds', first appeared in the 12th century when the Seljuk prince Saandjar established a province with that name, approximately corresponding to the present day Kordestan in Iran. However, it was not until the sixteenth century that the term became more widely applied to Kurdish principalities in general. Although Kurdistan has appeared on some maps since the sixteenth century, it should not be seen solely as a geographic term but also as a living cultural identity connected to this land.

1.2.2 Where is Kurdistan

The geographic boundaries of Kurdistan have fluctuated over time, but the region broadly spans the mountainous areas where the borders of Iraq, Iran, Syria, and Turkey converge. Its core lies along the Taurus and Zagros mountain chains and stretches southward to the Mesopotamian plain and northward to the plateaus of Armenian Anatolia (McDowall,2004.). Smaller Kurdish-populated areas near the Armenian and Azerbaijani borders with Turkey and Iran are sometimes referred to as "Red Kurdistan". Despite this, no universally accepted map of Kurdistan exists. Its borders remain undefined and disputed—Turkey has historically denied its existence, while Iran and Iraq downplay its size, and Syria denies any part of its territory is Kurdish (McDowall,2004.).

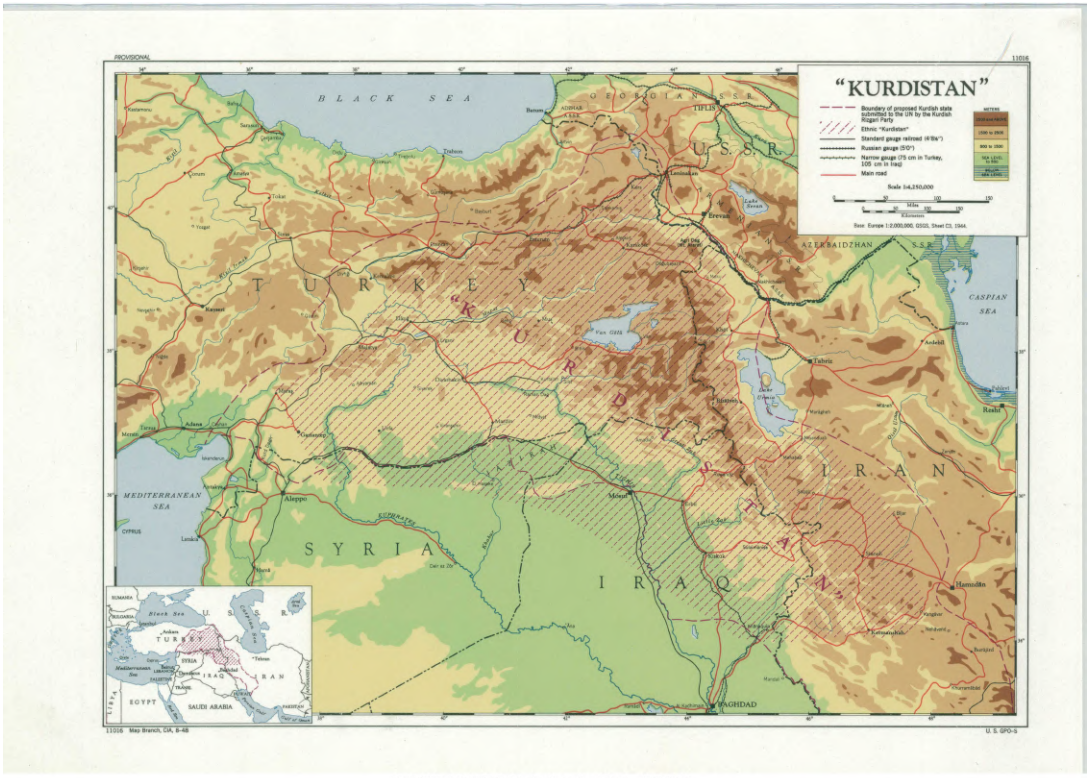

DECLASSIFIED Authority E.O. 13526
NND 76630

(a) Historic CIA map of Kurdistan (1948), showing proposed boundaries and Kurdish population concentrations.

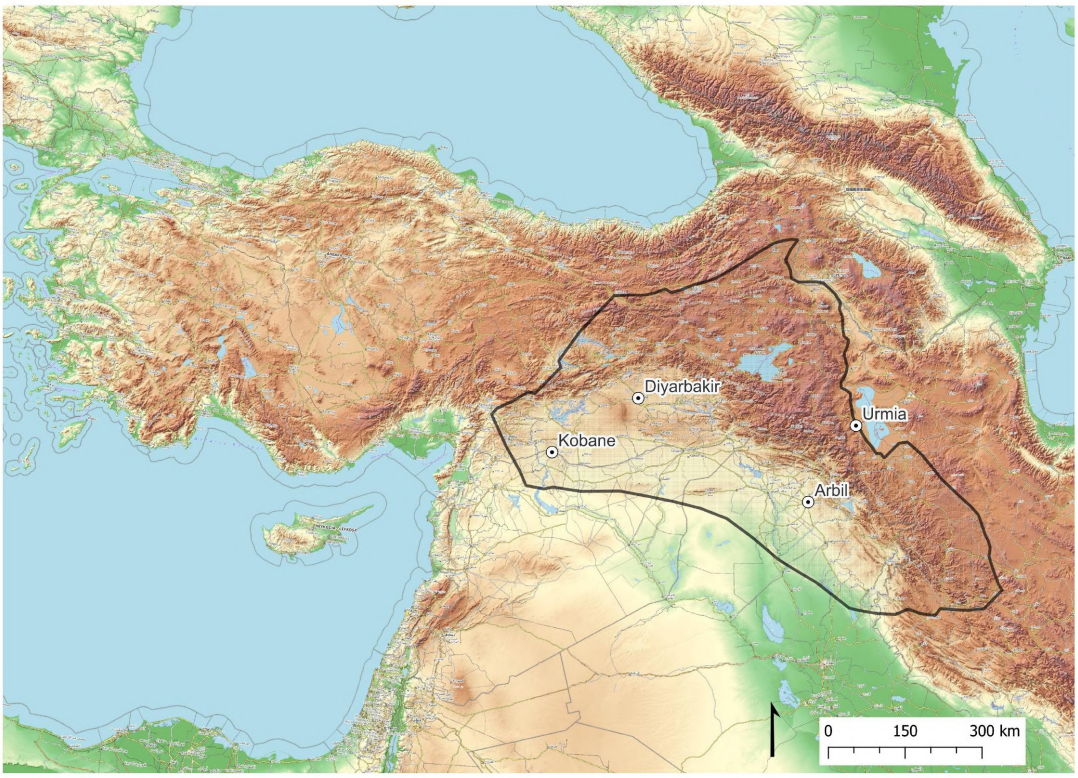

(b) Topographic map of Kurdistan (2025), created using QGIS and showing current terrain and urban centers.

Figure 1.2: Comparative cartography of Kurdistan: historical boundaries (top) and modern terrain (bottom).

1.2.3 Demographic Profile of Kurdistan

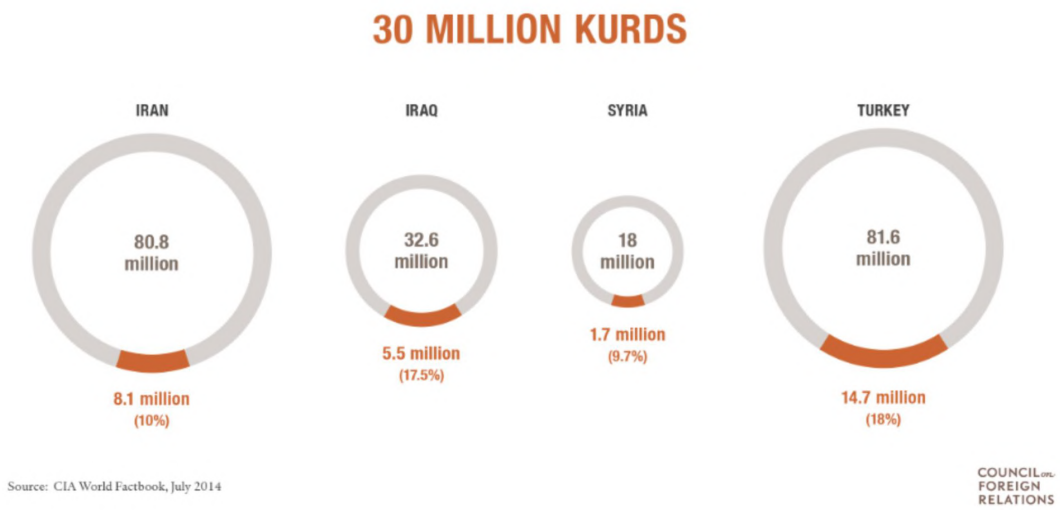

Figure 1.3: Estimated Kurdish population in Iran, Iraq, Syria, and Turkey.Rojhelat (Eastern Kurdistan in Iran), Bashur (Southern Kurdistan in Iraq), Rojava (Western Kurdistan in Syria), and Bakur (Northern Kurdistan in Turkey). Source: CIA World Factbook, July 2014; Council on Foreign Relations.

Today the Kurds number more than 40 million people, making them the largest stateless nation in the world. The great majority of Kurds live in a contiguous area that stretches across southeastern Turkey, northern Syria, northern Iraq and north-western Iran—a region commonly referred to as Kurdistan. This area has never been a sovereign Kurdish state, but has remained the historical homeland of the Kurdish people .

In Turkey, the Kurds number between 15 and 20 million people, and account for approximately 23% of the population. Most of them live in the south-eastern provinces, although large Kurdish communities also live in the large western cities of Istanbul, Izmir, Mersin and Adana. Since the 1980s, internal migration, as well as the destruction of Kurdish villages by the Turkish army in the 1990s, has caused a massive exodus of Kurds from the southeast to the western parts of the country.

In Iran, there are about 12 million Kurds, around 15% of the population. Most Iranian Kurds live in the provinces of Kurdistan, Kermanshah, Ilam and Western Azerbaijan. In Iraq, the Kurdish population is estimated to be between 6 and 7 million people, and they represent 17 to 20% of the country's population. The three provinces of Erbil, Duhok and Sulaymaniyah form the core of the Kurdish autonomous region. In Syria, Kurds are believed to number approximately 2.5 million people, or 15% of the population. Most Syrian Kurds live in the

north-eastern part of the country, especially in the region of Jazira (Hasakah governorate), as well as in Afrin and Kobani .

Outside the Middle East, the Kurdish diaspora is estimated at more than 2 million people. The largest communities are in Germany (800,000–1 million), France (200,000), Sweden (130,000), the Netherlands (100,000), the UK (70,000), and Switzerland (60,000). Smaller communities exist in the US, Canada, Australia, and the former Soviet Union.

The Kurds speak several dialects of the Kurdish language, mainly Kurmanji in the north and Sorani in the south, and also Zazaki and Gorani. Most Kurds are Sunni Muslims of the Shafi'i school, but there are also many Alevi Kurds (especially in Turkey), as well as followers of other religions, such as Yazidism, Yarsanism (Ahl-e Haqq), Christianity and Shi'a Islam.

Today, the great majority of Kurds live in cities. Large Kurdish cities include Diyarbakir (Turkey), Erbil and Sulaymaniyah (Iraq), Sanandaj and Mahabad (Iran), and Qamishli (Syria). The Kurds have experienced forced displacement, war and economic migration, which have contributed to high levels of urbanization across the region.

Despite their large numbers and ancient presence in the Middle East, the Kurds have remained a stateless nation. They have long struggled for the recognition of their cultural and political rights in each of the four states where they live. Kurdish identity and demands have often been met with repression, forced assimilation and denial of existence.

1.2.4 Why Kurdistan

Kurdistan presents a compelling case for research on climate extremes and heatwaves due to its underrepresentation in global climate studies, complex topography, and increasing environmental vulnerability. Despite being home to nearly 30 million people across several nation-states, the region has received limited attention in climate science, particularly in terms of localized heatwave mapping, environmental risk, and adaptation strategies. This lack of research represents a critical gap in understanding the implications of climate change in semi-arid and geopolitically sensitive regions.

Kurdistan is characterized by a highly varied landscape, a mix of extensive plateaus, high-altitude plains, and rugged mountain ranges such as the Zagros and Taurus Mountains, which create diverse climatic zones across its territory. These variations influence local microclimates, land use, and population vulnerability. The mountainous terrain also shapes water availability, agriculture, and settlement patterns, making it particularly susceptible to the compounded impacts of climate variability, land degradation, and geopolitical fragmentation (Kurdistan Regional Government, 2025).

In addition to its environmental diversity, the geopolitical fragmentation of Kurdistan—divided across Turkey, Iraq, Iran, Syria, and parts of Armenia—has impeded unified climate action, particularly in regions with weak governance or lacking transboundary coordination. Historical border divisions not only denied the Kurdish population a sovereign nation but also created administrative discontinuities that limit integrated environmental planning and climate resilience. This fragmentation contributes to what scholars and activists describe as the invisibility of Kurds in environmental governance frameworks, where their climate-related challenges are frequently overlooked or dismissed by central governments.

In the Autonomous Administration of North and East Syria (Rojava), environmental governance is grounded in a constitutional commitment to sustainability. Environmental protection and the sustainable development of natural ecosystems are regarded as moral and sacred national duties. The society is defined as an ecological democratic society. Preserving environmental life and the ecosystem is recognized as a duty of citizens, society, and all institutions. Natural resources are defined as the property of society and are to be used in a fair and sustainable way, aligning ecological protection with principles of social equity and grassroots democracy (Rojava Information Center, 2023). These provisions make Rojava a rare example of a stateless, community-led administration that integrates environmental stewardship as a foundational pillar of governance.

1.3 General Aim

Given the increasing impacts of climate extremes in the Middle East, this study aims to systematically analyze, map, and interpret heatwaves and extreme temperature events in the geopolitical region of Kurdistan, spanning parts of Iran, Iraq, Turkey, and Syria. By integrating geospatial analysis, climatological datasets, and land cover data, the research will assess both the spatial and temporal dynamics of extreme heat and their interactions with urbanization, land use, and ecological patterns. This interdisciplinary approach seeks to provide a comprehensive understanding of the behavior of heat waves, their influence on urban and rural landscapes, and the implications for environmental sustainability and human well-being.

1.3.1 Specific Aims

This research aims to detect and quantify the occurrence of heatwaves and extreme temperature events across the Kurdistan region using historical climate datasets such as CMIP6 and ERA5. By applying scientifically robust thresholds, such as the 90th percentile, the study will distinguish extreme heat events from normal temperature fluctuations. In addition, the project will

analyze the spatial distribution of Land Surface Temperature (LST) across urban and rural areas using satellite imagery from Earth Explorer, identifying thermal anomalies and urban heat island (UHI) effects. To deepen the analysis, land cover data from sources like ESA WorldCover 10m will be integrated with LST measurements to explore the relationship between land surface characteristics and local temperature dynamics. This land cover analysis will help assess how ecological patterns, such as vegetation density, urbanization, and bare land, affect heat retention and distribution throughout the region. Furthermore, the study will evaluate the socioeconomic implications of extreme heat, with a focus on vulnerable populations, infrastructure, and geopolitical divisions within Kurdistan. The final objective is to produce comprehensive geospatial maps and visualizations that integrate climate, land cover, and socioeconomic data, offering evidence-based insights to support urban planning, climate adaptation, and policy development to meet the needs of heat.

2 Data and Methods

2.1 Data Collection

2.1.1 Study Cases in Kurdistan

This study focuses on four urban areas located within the broader Kurdistan region: Kobani (Syria), Diyarbakır (Turkey), Erbil (Iraq), and Urmia (Iran). These cities were selected due to their geographic diversity, climate vulnerability, and socio-political complexity. Each represents a unique intersection of urban development, environmental stress, and exposure to extreme heat events. Their inclusion provides a regionally balanced framework for comparative spatial analysis of land surface temperature (LST) and urban heat island (UHI) effects.

Kobani (Syria) Kobani is a small city in the Aleppo governorate of northern Syria, covering approximately 7 km². Before the Syrian civil war, it had a population of around 60,000 and approximately 90% of the inhabitants were Kurds, with the remaining 10% comprising Arabs, Turkmen, and Armenians. Years of armed conflict have caused extensive damage to the infrastructure and contamination with unexploded ordnance, placing returning residents at continued risk. Due to the lack of an official administrative boundary, the urban extent of Kobani was manually digitized in QGIS using high-resolution satellite imagery and OpenStreetMap features. According to Köppen–Geiger climate classifications, Kobani falls within a cold semi-arid zone (BSk), characterized by hot, dry summers and cool winters (Beck et al., 2018). These conditions, combined with post-conflict degradation and minimal vegetation, make Kobani highly susceptible to heat exposure.

Diyarbakır (Turkey) Diyarbakr is located in southeastern Turkey along the Tigris River and is the capital of Diyarbakır Province. It spans approximately 15,058 km², with an estimated population of 1.82 million as of 2023 (CityPopulation.de, 2025). The city is predominantly Kurdish,approximately 80% with historical Assyrian and Armenian minorities. The climate

of Diyarbakr is classified as semi-arid hot (BSh), with very hot summers, mild winters, and low annual precipitation (Beck et al., 2018). Rapid urban growth, limited vegetative cover, and socio-economic disparities have contributed to the formation of pronounced urban heat island effects, particularly in the densely built city core. The Kurdish population of the city continues to face historical marginalization, affecting access to infrastructure and adaptation planning.

Erbil (Iraq) Erbil (also known as Hawler) is the capital of the Kurdistan region in Iraq, with a population of approximately 1.43 million and a land area of 14,471 km² (KRG, 2025). Approximately 93% of its residents are Kurds, with minorities including Turkmen, Assyrians, and Arabs. Erbil lies within a transitional climate zone between Mediterranean (Csa) and hot semi-arid (BSh) types, featuring extremely hot, dry summers and short, mild winters (Beck et al., 2018). The city has undergone rapid spatial expansion due to displacement-driven population growth and real estate development. This has led to widespread loss of green spaces and increased impervious surfaces, intensifying heat retention, and reducing resilience to thermal extremes. The absence of water bodies and uneven urban planning further exacerbate localized heat risks.

Urmia (Iran) Urmia is the capital of the West Azerbaijan province in northwest Iran and had a recorded population of 736,224 in 2016 (CityPopulation.de, 2025). It is an ethnically diverse city, home to Iranian Azerbaijanis, Kurds, Assyrians, and Armenians. The Kurdish population in Urmia, Iran, is estimated to be between 15% and 20% of the total population of the city. significant presence of Kurds, particularly in the surrounding rural areas. The Herki Kurds, a subgroup of Kurmanji speakers, are notably present in the western countryside of Urmia, including the Targavar and Margavar valleys. Urmia has a cold semi-arid climate (BSk), with hot, dry summers and cold winters (Beck et al., 2018). The city's proximity to ecologically stressed Lake Urmia, once the largest saltwater lake in the Middle East, increases its environmental vulnerability. The shrinking of the lake due to overextraction and climate stress has altered local humidity and surface albedo, amplifying the impacts of urban heat. Combined with uneven infrastructure development, Urmia provides a critical case for assessing the interaction between ecological degradation and urban thermal behavior.

2.1.2 Land Cover Data

Land cover analysis in this study utilized the ESA WorldCover 10 m 2021 v200 product, developed under the European Space Agency's 5th Earth Observation Envelope Programme (EOEP-5). This dataset provides a global land cover map at 10-meter resolution, derived from Sentinel-1 and Sentinel-2 satellite imagery. According to the official user manual, the dataset offers a discrete classification map with 11 land cover classes, defined using the FAO's Land Cover Classification System (LCCS) (Zanaga et al., 2022). The 11 classes include: Tree cover, Shrubland, Grassland, Cropland, Built-up, Bare/Sparse vegetation, Snow and Ice, Permanent water bodies, Herbaceous Wetland, Mangroves, and Moss and Lichen. Each class is assigned a unique digital number (DN), which facilitates classification and spatial analysis (Zanaga et al., 2022). For this research, the relevant WorldCover tiles covering the cities of Erbil, Urmia, Diyarbakir, and Kobani were downloaded. Using QGIS, these were clipped to 20 km radius buffers centered on each urban area. The rasters were vectorized, reclassified by DN value, and quantified using area statistics (in square kilometers). The resulting land cover distributions were then linked with land surface temperature (LST) and hot day frequency data to assess the relationship between land cover and thermal exposure.

Map code	Land Cover Class	LCCS code	Definition	Color code (RGB)
10	Tree cover	A12A3 // A11A1 A24A3C1(C2)-R1(R2)	This class includes any geographic area dominated by trees with a cover of 10% or more. Other land cover classes (shrubs and/or herbs in the understorey, built-up, permanent water bodies, ...) can be present below the canopy, even with a density higher than trees. Areas planted with trees for afforestation purposes and plantations (e.g. oil palm, olive trees) are included in this class. This class also includes tree covered areas seasonally or permanently flooded with fresh water except for mangroves.	0,100,0
20	Shrubland	A12A4 // A11A2	This class includes any geographic area dominated by natural shrubs having a cover of 10% or more. Shrubs are defined as woody perennial plants with persistent and woody stems and without any defined main stem being less than 5 m tall. Trees can be present in scattered form if their cover is less than 10%. Herbaceous plants can also be present at any density. The shrub foliage can be either evergreen or deciduous.	255, 187, 34
30	Grassland	A12A2	This class includes any geographic area dominated by natural herbaceous plants (Plants without persistent stem or shoots above ground and lacking definite firm structure): (grasslands, prairies, steppes, savannahs, pastures) with a cover of 10% or more, irrespective of different human and/or animal activities, such as: grazing, selective fire management etc. Woody plants (trees and/or shrubs) can be present assuming their cover is less than 10%. It may also contain uncultivated cropland areas (without harvest/ bare soil period) in the reference year	255, 255, 76
40	Cropland	A11A3(A4)(A5) // A23	Land covered with annual cropland that is sowed/planted and harvestable at least once within the 12 months after the sowing/planting date. The annual cropland produces an herbaceous cover and is sometimes combined with some tree or woody vegetation. Note that perennial woody crops will be classified as the appropriate tree cover or shrub land cover type. Greenhouses are considered as built-up.	240, 150, 255
50	Built-up	B15A1	Land covered by buildings, roads and other man-made structures such as railroads. Buildings include both residential and industrial building. Urban green (parks, sport facilities) is not included in this class. Waste dump deposits and extraction sites are considered as bare.	250, 0, 0
60	Bare / sparse vegetation	B16A1(A2) // B15A2	Lands with exposed soil, sand, or rocks and never has more than 10 % vegetated cover during any time of the year	180, 180, 180
70	Snow and Ice	B28A2(A3)	This class includes any geographic area covered by snow or glaciers persistently	240, 240, 240
80	Permanent water bodies	B28A1(B1) // B27A1(B1)	This class includes any geographic area covered for most of the year (more than 9 months) by water bodies: lakes, reservoirs, and rivers. Can be either fresh or salt-water bodies. In some cases the water can be frozen for part of the year (less than 9 months).	0, 100, 200
90	Herbaceous wetland	A24A2	Land dominated by natural herbaceous vegetation (cover of 10% or more) that is permanently or regularly flooded by fresh, brackish or salt water. It excludes unvegetated sediment (see 60), swamp forests (classified as tree cover) and mangroves see 95)	0, 150, 160
95	Mangroves	A24A3C5-R3	Taxonomically diverse, salt-tolerant tree and other plant species which thrive in intertidal zones of sheltered tropical shores, "overwash" islands, and estuaries.	0, 207, 117
100	Moss and lichen	A12A7	Land covered with lichens and/or mosses. Lichens are composite organisms formed from the symbiotic association of fungi and algae. Mosses contain photo-autotrophic land plants without true leaves, stems, roots but with leaf-and stemlike organs.	250, 230, 160

Figure 2.1: ESA WorldCover land cover classification table (v2.0), including map codes, class names, definitions, and RGB color codes.

2.1.3 Climate Data (CMIP6 and ERA5)

The climate data used in this study were sourced from two primary datasets: CMIP6 (Coupled Model Intercomparison Project Phase 6) and ERA5. CMIP6 provides multimodel climate projections under various Shared Socioeconomic Pathway (SSP) scenarios, enabling the assessment of future temperature extremes and long-term climate risks. ERA5, produced by the Copernicus Climate Change Service (C3S), offers high-resolution hourly reanalysis data of atmospheric variables from 1979 onward, serving as a robust historical reference. These datasets were accessed via the Copernicus Climate Data Store (CDS) and selected for their high temporal and spatial resolution, consistency across regions, and compatibility with geospatial workflows such as QGIS. ERA5 provides past temperature records that enable direct comparison with CMIP6 projections, supporting historical-to-future trend analysis. While NOAA NCEI datasets were considered during preliminary review, ERA5 and CMIP6 were prioritized for their superior data quality and integration potential. Selected variables included daily maximum 2m air temperature, analyzed across four key sites: Diyarbakir, Kobani, Urmia, and Erbil. The use of these datasets ensures methodological rigor and spatial consistency in evaluating heatwaves and climate extremes in the Kurdistan region.

2.1.4 Climate Data Selection and Configuration

To analyze extreme heat events, daily maximum temperature data were obtained from the CMIP6 historical ensemble, accessed via the Copernicus Climate Data Store. The selected data covered the summer months (June, July, August) from 1991–2020 and the year 2024, at a daily temporal resolution. This time scale was essential for identifying extreme heat days using the 90th percentile method. Only historical simulations were used; no future climate scenarios (SSPs) were included in the analysis. The data were processed for four urban areas—Diyarbakır, Kobani, Urmia, and Erbil—and clipped to 20 km buffers around each city for spatial analysis.

Selected Geographical Area:

Figure 2.2: Map of the Kurdistan region showing the selected study cities: Diyarbakır, Kobani, Urmia, and Erbil.

- Diyarbakir, Turkey: 37.9147° N, 40.2312° E
- Kobani, Syria: 36.8706° N, 38.4244° E
- Urmia, Iran: 37.5510° N, 45.0750° E
- Erbil, Iraq: 36.1911° N, 44.0094° E

Following selection of temporal resolution, variable, models, and regions, the data set request was validated to ensure consistency. This resulted in a high-resolution dataset comprising daily maximum temperature values from the historical period (1991–2020) and the year 2024. These data formed the foundation for the threshold and heatwave analyses conducted in this study.

2.1.5 Land Surface Temperature and Urban Heat Island calculation

Land Surface Temperature (LST) is a fundamental parameter in understanding surface energy balance and thermal behavior across urban and rural environments. As Weng (2009) explains, LST is an important parameter in the studies of urban thermal environment and dynamics. LST modulates the air temperature of the lower layer of urban atmosphere, and is a primary factor in determining surface radiation and energy exchange, the internal climate of buildings, and human comfort in the cities. Its ability to reveal spatial temperature variations makes it especially useful for detecting urban heat islands and extreme heat zones, which are central to this study. In this research, LST data were acquired from Landsat 8 and Landsat 9 surface temperature products provided by the U.S. Geological Survey (USGS) through the Earth Explorer platform. The datasets used were Collection 2 Level-2 products, which include surface temperature (ST) bands processed with atmospheric correction and emissivity standardization. No custom NDVI or emissivity modeling was conducted, as the analysis relies on the standardized, validated LST values provided by USGS. The spatial resolution of these datasets is 30 meters, making them suitable for regional analysis of urban and peri-urban heat distribution. These maps were generated using QGIS to visualize and classify the LST raster data into meaningful thermal categories. Thermal infrared remote sensing enables such surface heat assessments even in data-scarce regions. As noted by Weng (2009), Remotely sensed TIR data are a unique source of information to define surface heat islands, which are related to canopy layer heat islands (p. 336). This capability is especially important for the Kurdistan region, where field-based climate data are sparse or inconsistent across borders. In this study, the LST datasets served as a basis for analyzing spatial heat patterns in Diyarbakir, Kobani, Erbil, and Urmia, contributing to the broader objective of mapping extreme heat events and assessing their relation to land cover, urban expansion, and vulnerability. Thermal infrared data used for LST analysis were obtained from Landsat 8 and Landsat 9 via the USGS Earth Explorer platform. Specifically, Surface Temperature Band 10 (`ST_B10`) from Level-1 imagery was used, stored in GeoTIFF (`.tiff`) format.

The Landsat thermal bands were converted from Digital Number (DN) values to Kelvin temperatures using the following radiometric conversion formula:

$$\text{Surface Temperature (K)} = 0.00341802 \times \text{DN} + 149.0 \tag{2.1}$$

This equation, derived from USGS calibration metadata, transforms raw radiance data into physical temperature measurements suitable for geospatial analysis. The resulting LST rasters were clipped using the 20 km urban buffers surrounding Erbil, Diyarbakır, Kobani, and Urmia. LST layers were then classified into temperature intervals to identify heat intensity patterns and

support comparative analysis.

The Urban Heat Island (UHI) effect was evaluated using absolute LST values from Landsat 8 and 9, rather than the ΔT method, which compares urban temperatures to rural baselines. Due to inconsistencies in land cover and the absence of uniformly defined rural zones in some case studies, ΔT was not feasible. Instead, absolute temperature maps allowed for intra-urban comparisons of thermal exposure. Classified heatmaps were used to detect hotspots and anomalies during the summer of 2024, supporting the spatial analysis of urban heat intensity.

2.1.6 QGIS and Satellite Imagery (Earth Explorer)

The geospatial analyses in this study were conducted using `QGIS` (Quantum Geographic Information System), version 3.16.1, developed by the QGIS Development Team [**?**]. QGIS is an open-source, cross-platform GIS software distributed under the GNU General Public License (GPL). It supports a broad range of spatial data formats, offers an extensible plugin architecture, and is widely used in academic and professional applications for spatial analysis, data integration, and cartographic visualization. In this research, QGIS functioned as the primary analytical platform for handling both raster and vector datasets, including Land Surface Temperature (LST), land cover, and socioeconomic overlays.

Raster data were georeferenced and preprocessed to ensure spatial consistency with other datasets. For vector data, shapefiles representing urban boundaries, 20 km buffer zones, and administrative areas were used, including associated attribute tables (`.dbf`), spatial indices (`.shx`), and projection files (`.prj`).

QGIS also facilitated the integration of socioeconomic datasets, including population density and land use, to assess the vulnerability of different communities to extreme heat. These datasets were overlaid on LST heatmaps to identify spatial intersections between heat exposure and social risk factors. This overlay approach enhances understanding of climate vulnerability at the neighborhood scale and supports targeted recommendations for climate adaptation and urban resilience planning.

Kobani Boundary Digitization: Due to the absence of an officially recognized administrative boundary for Kobani in public geospatial databases, no formal shapefiles or cadastral maps were available. To address this, the boundary used in this study was manually digitized using QGIS software, with OpenStreetMap as the primary basemap. The boundary was delineated by tracing urban and peri-urban features visible in satellite imagery and road networks. Although

care was taken to ensure spatial accuracy, the result should be considered an approximation due to the political and administrative complexity of the region.

2.2 GIScience Approach

This study applied a Geographic Information Science (GIScience) framework to investigate the spatial dynamics of heatwaves and land surface temperature variations in selected cities of the Kurdistan region. Rather than focusing on theoretical or participatory GIS models, the research adopted a data-driven, remote-sensing-based approach using established geospatial tools and publicly available datasets. All spatial analyses were performed in QGIS, an open-source geographic information system, which served as the primary platform for processing raster and vector data. The study integrated multiple spatial datasets including Landsat 8 and 9 thermal imagery for Land Surface Temperature (LST) analysis, ESA WorldCover 10m data for land cover classification, and historical climate datasets from ERA5 and CMIP6. These were used to map surface heat anomalies, classify land cover types, and analyze spatial patterns in urban and peri-urban areas. Buffer zones with a 20 km radius were generated around each case study city to define the extent of spatial analysis. Within these buffers, raster data were clipped, vectorized, reclassified, and statistically analyzed using tools such as zonal statistics and classification overlays. This allowed for comparative analysis of surface temperature patterns across different land cover categories and between the four urban environments. In the case of Kobani, where no official shapefiles or administrative boundaries were available, the urban extent was manually digitized in QGIS using visual interpretation of satellite imagery with OpenStreetMap as a supporting basemap. However, this study did not involve any Volunteered Geographic Information (VGI) or participatory data collection. No new data were contributed to OpenStreetMap or other platforms, and no community-based mapping or citizen input was used. All data sources were secondary, open-access datasets used solely for analysis purposes. GIScience in this study was applied as a methodological foundation to quantify and visualize the relationship between extreme heat events, land cover composition, and urban structure. The integration of satellite remote sensing, spatial statistics, and climate thresholds allowed for localized assessments of urban heat vulnerability in a geopolitically fragmented and ecologically sensitive region.

2.3 Data Analysis

To truly grasp and visualize the impact of heatwaves and climate extremes, we need a structured, data-driven approach that brings together multiple analytical methods. Heatwaves are not

just meteorological events; they carry significant consequences for ecosystems, economies, and human well-being (IPCC, 2021). Understanding their frequency, intensity, and spatial distribution is essential for developing mitigation strategies and fostering climate resilience (Perkins Alexander, 2013). In this study, we analyze both historical climate data (from 1991 to 2020) and the latest temperature records from 2024 to track trends in extreme heat across the Kurdistan region, focusing on Diyarbakir, Kobani, Urmia, and Erbil. These locations, each with unique climatic and geographical characteristics, offer critical insights into how rising temperatures are manifesting across diverse landscapes, from urban centers to agricultural zones (Harrington Otto, 2020). The selection of this time frame aligns with previous climate studies, where long-term datasets allow for a clearer identification of trends in extreme weather events (IPCC, 2018). By blending statistical analysis, trend evaluation, geospatial mapping, and an assessment of socioeconomic impacts, this research aims to paint a clearer picture of how heatwaves are evolving and what that means for the people and landscapes of the region. Extreme heat events disproportionately affect vulnerable populations, including the elderly, children, and low-income communities, who may lack access to adequate cooling systems or healthcare facilities (Smith et al., 2020). Beyond identifying patterns in temperature extremes, this approach helps pinpoint high-risk areas, assess potential threats to public health and food security, and understand how infrastructure and daily life are being impacted by rising temperatures (World Meteorological Organization, 2022). Moreover, mapping these climate extremes enables policymakers, urban planners, and environmental organizations to make informed decisions, whether it's about designing heat-resistant infrastructure, implementing early warning systems, or developing adaptive agricultural techniques (Field et al., 2012). The integration of geospatial analysis with climate data allows for a more localized understanding of heatwave intensity, making it possible to craft targeted interventions that address the most at-risk populations (Huang et al., 2019). For example, urban centers like Erbil and Diyarbakir experience exacerbated heatwave effects due to the UHI phenomenon, which results in significantly higher temperatures compared to surrounding rural areas (Stone et al., 2010). As climate change continues to accelerate, the need for such comprehensive analysis becomes increasingly urgent. The findings from this study not only contribute to the scientific understanding of heatwave dynamics but also serve as a foundation for climate adaptation efforts in the region, ensuring that communities can better prepare for and respond to the growing challenges posed by extreme heat (IPCC, 2021). By utilizing interdisciplinary approaches and integrating environmental, economic, and social data, this research provides a critical framework for assessing climate extremes and guiding future resilience-building initiatives (Haines et al., 2006).

2.3.1 Climate extreme calculation in Python

To detect extreme heat events in each case study location, this research employed a threshold-based classification method using the 90th percentile of historical daily maximum temperatures. Percentiles are used as an indicator of the likelihood of a particular event. The percentile refers to the ranking of a particular value relative to all of the values for that site. For example, if there were 100 temperature values recorded for a site, we could place them in order from the coolest to the warmest temperature. Of these values, the 10th lowest value would be called the 10th percentile and the 20th lowest value the 20th percentile. This is applied right up until the 100th percentile, which includes all of the values that have been measured for that site, and is equal to the highest temperature value.(Australian Bureau of Meteorology, n.d.) Historical daily maximum temperature data for the summer season (JJA: June, July, August) from 1991 to 2020 were extracted using the CMIP6 climate model ensemble. For each city, the 90th percentile value was calculated from this dataset. The resulting threshold was then used to classify 2024 daily maximum temperature records into two categories: Non-extreme (below the 90th percentile)

Extreme heat days (at or above the 90th percentile)

All calculations were performed using Python with the Pandas and NumPy libraries for time-series filtering and statistical analysis. These thresholds were later used in Section 3 to evaluate the frequency, intensity, and duration of extreme heat events in the study region.

2.3.2 Hot Day Frequency and Duration

Following the threshold calculation, daily temperature records for the year 2024 were analyzed to identify ”hot days,” defined as those exceeding the respective 90th percentile threshold for each city. Python scripts were used to flag these dates and count their frequency across the summer months (JJA). To analyze the persistence of heat events, sequences of consecutive hot days were identified and grouped to define heatwaves. A heatwave was classified as any period with three or more consecutive hot days. For each city, the frequency of hot days, number of heatwave episodes, and the duration of each heatwave were recorded. Based on the timing of identified hot days, Landsat 8 and 9 satellite imagery was selectively acquired to correspond with peak temperature events. This allowed for targeted analysis of LST in QGIS, ensuring that remote sensing evaluation was aligned with the most thermally extreme periods. This analysis allows for direct comparison between cities in terms of their exposure to extreme heat during 2024, and provides a basis for evaluating temporal trends and the potential intensification of heatwaves relative to historical patterns.

2.3.3 LST–Land Cover Relationship

To investigate how land surface characteristics affect heat distribution, LST data were derived from Landsat 8 and 9 thermal imagery (Band 10: `ST_B10`) for the specific hot days identified in each city. These thermal images were processed in `QGIS` to convert digital numbers (DN) into temperature values using the appropriate calibration formula. Resulting LST rasters were clipped to both the municipal boundaries and 20 km urban buffer zones to compare urban cores with peri-urban conditions across all case studies.

In parallel, ESA *WorldCover 10m* land cover maps were reclassified according to major surface types such as built-up, cropland, grassland, shrubland, and bare soil. These maps were vectorized and overlaid with the LST rasters.

Using QGIS tools including *Zonal Statistics* and *Statistics by Categories*, average LST values were calculated for each land cover class. This spatial analysis helped identify which land cover types were associated with higher surface temperatures. The results informed the assessment of localized urban heat islands and supported the interpretation of how landscape composition influences thermal exposure.

3 Results and Discussion

3.1 Climatic analysis and identification of hotdays

This section presents the temperature thresholds derived from the 90th percentile of daily maximum temperatures during the summer season (June–August) for the historical baseline period of 1991–2020. These thresholds serve as critical benchmarks for detecting extreme heat events in 2024.

Thresholds were calculated for each city individually using CMIP6-based historical datasets. The 90th percentile value captures the hottest 10% of summer days over the 30-year period, reflecting local climatic norms and variability. The values were computed using Python's `NumPy` percentile function applied to daily maximum temperature data filtered by the JJA months.

City-Specific Thresholds

Table 3.1: 90th Percentile Summer Temperature Thresholds (1991–2020)

City	**90th Percentile Threshold (°C)**
Erbil	39.75
Diyarbakır	40.12
Kobani	39.45
Urmia	37.90

These values illustrate important regional differences. Diyarbakır exhibits the highest threshold, probably influenced by its continental climate and location in the inland. Urmia shows the lowest value, consistent with its elevation and proximity to water bodies.

Threshold Validation Plots

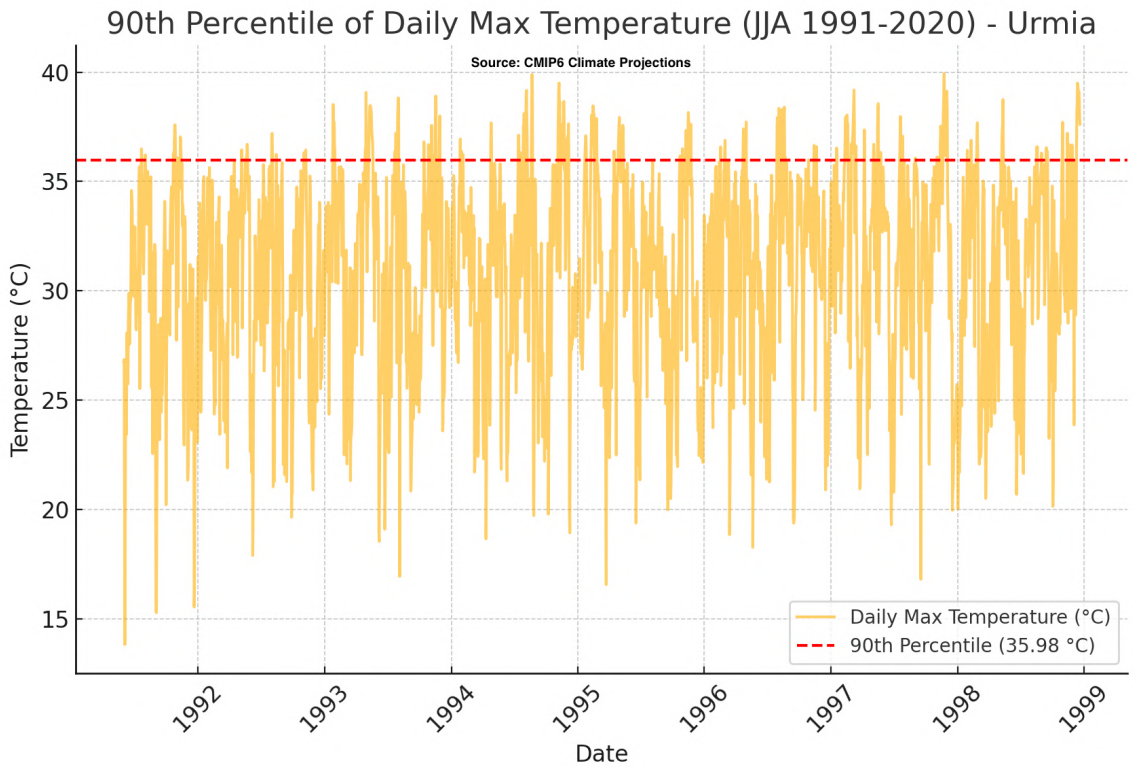

(a) 90th Percentile Threshold (1991–2020) – Urmia

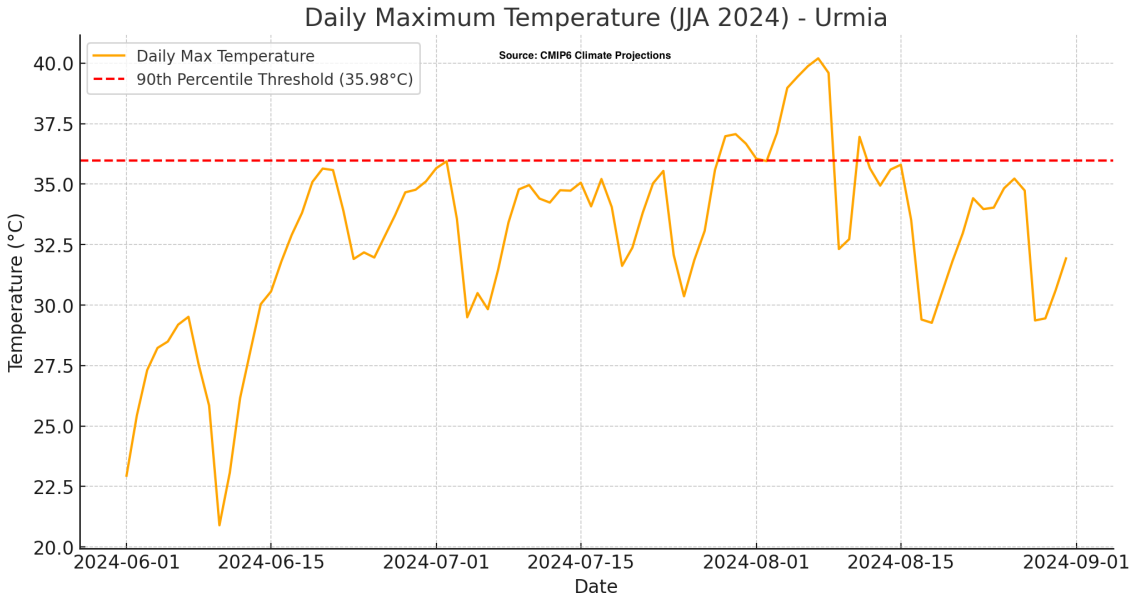

(b) Daily Max Temperatures – Summer 2024

Figure 3.1: Urmia: Threshold validation and 2024 summer temperature comparison

Urmia Panel (a) shows the 90th percentile threshold for daily maximum summer temperatures in Urmia, calculated as 35.98 ° C from the 1991-2020 data. This threshold is used to define heat extremes. Panel (b) compares the summer of 2024 against this benchmark, showing that many days in July and early August exceeded it. These validated heat events were used to select representative satellite imagery for land surface temperature (LST) analysis.

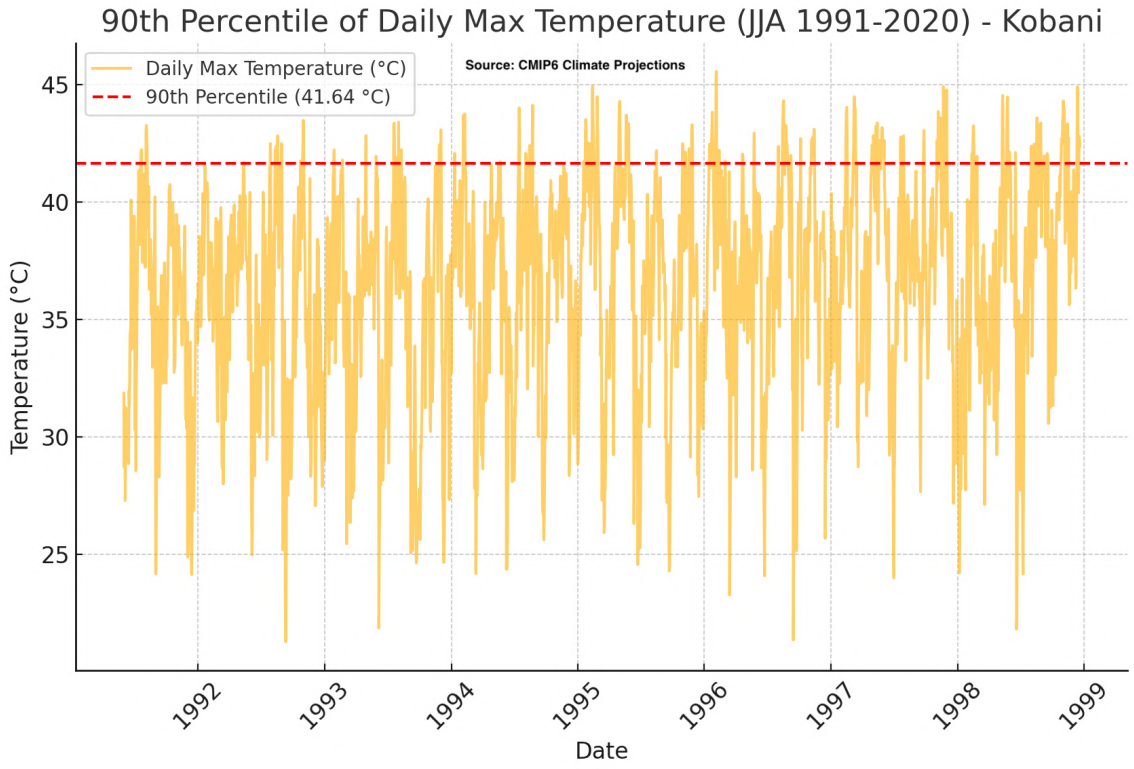

(a) 90th Percentile Threshold (1991–2020) – Kobani

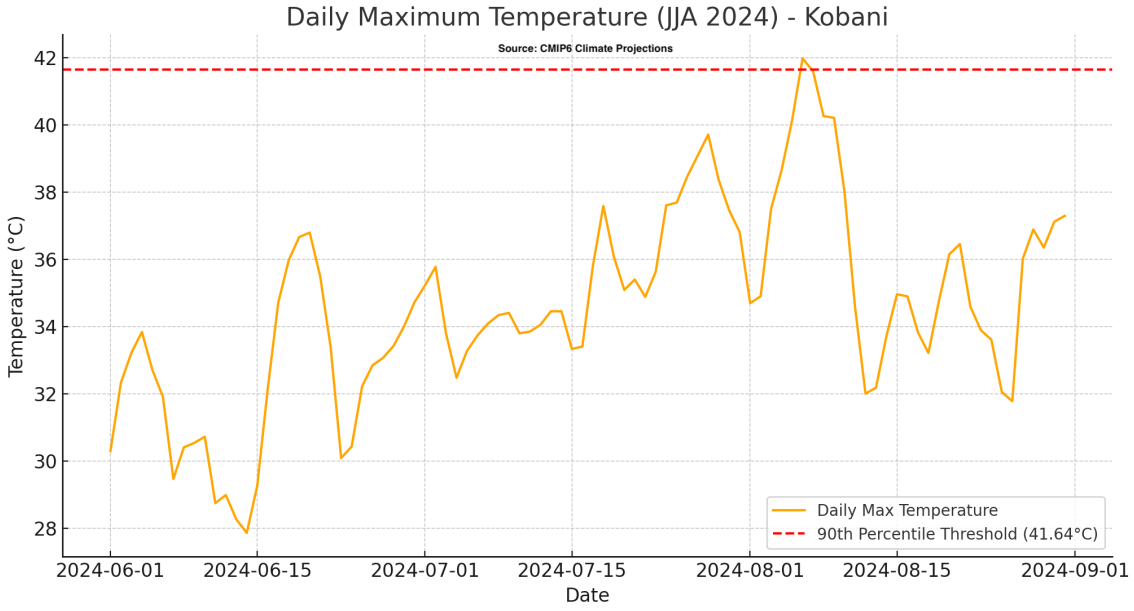

(b) Daily Max Temperatures – Summer 2024

Figure 3.2: Kobani: Threshold validation and 2024 summer temperature comparison

Kobani The historical threshold for Kobani (panel a) is set at 41.64°C based on 1991–2020 summer data. This high value reflects intense heat exposure. Panel (b) indicates that during 2024, particularly in mid-July and early August, maximum temperatures repeatedly exceeded

this benchmark. These days were flagged as heat events and used to anchor the thermal analysis of the city in satellite data.

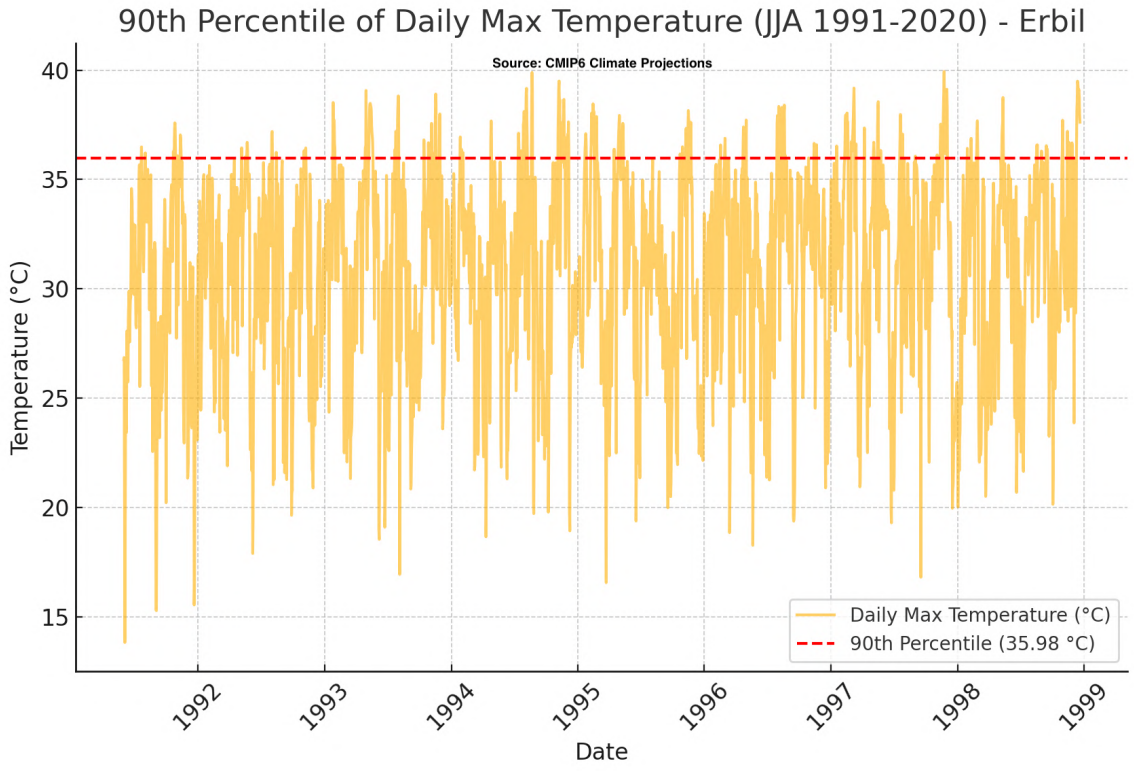

(a) 90th Percentile Threshold (1991–2020) – Erbil

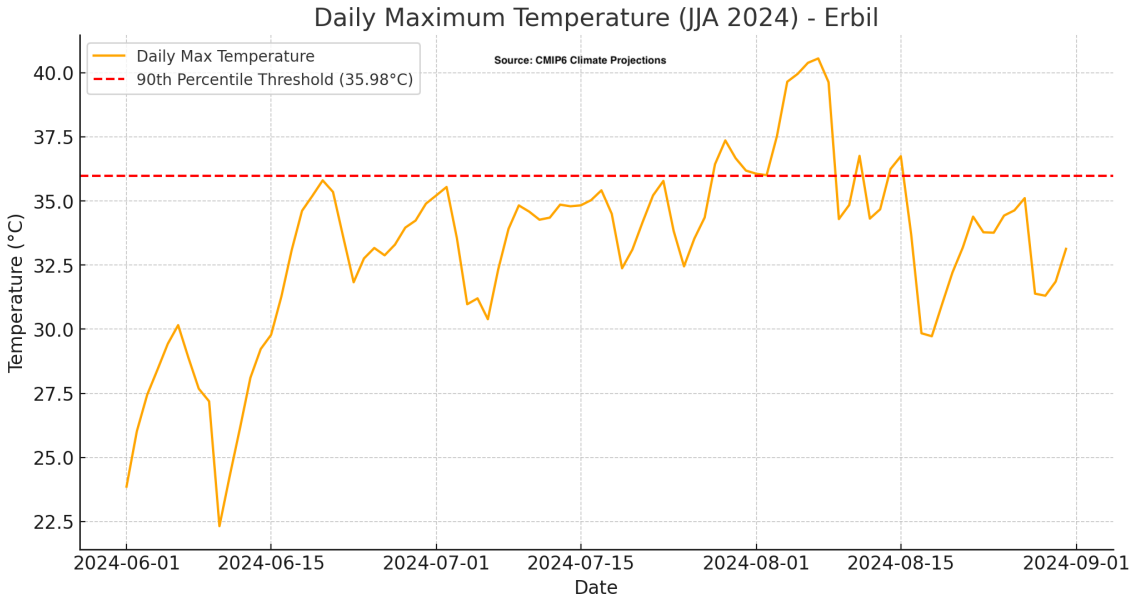

(b) Daily Max Temperatures – Summer 2024

Figure 3.3: Erbil: Threshold validation and 2024 summer temperature comparison

Erbil In Erbil, the 90th percentile value for summer maximum temperatures from 1991–2020 is 35.98°C, as shown in panel (a). This benchmark was exceeded on several days in summer 2024 (panel b), confirming multiple extreme heat days. These exceedances guided the selection of imagery for LST extraction and spatial heat assessment.

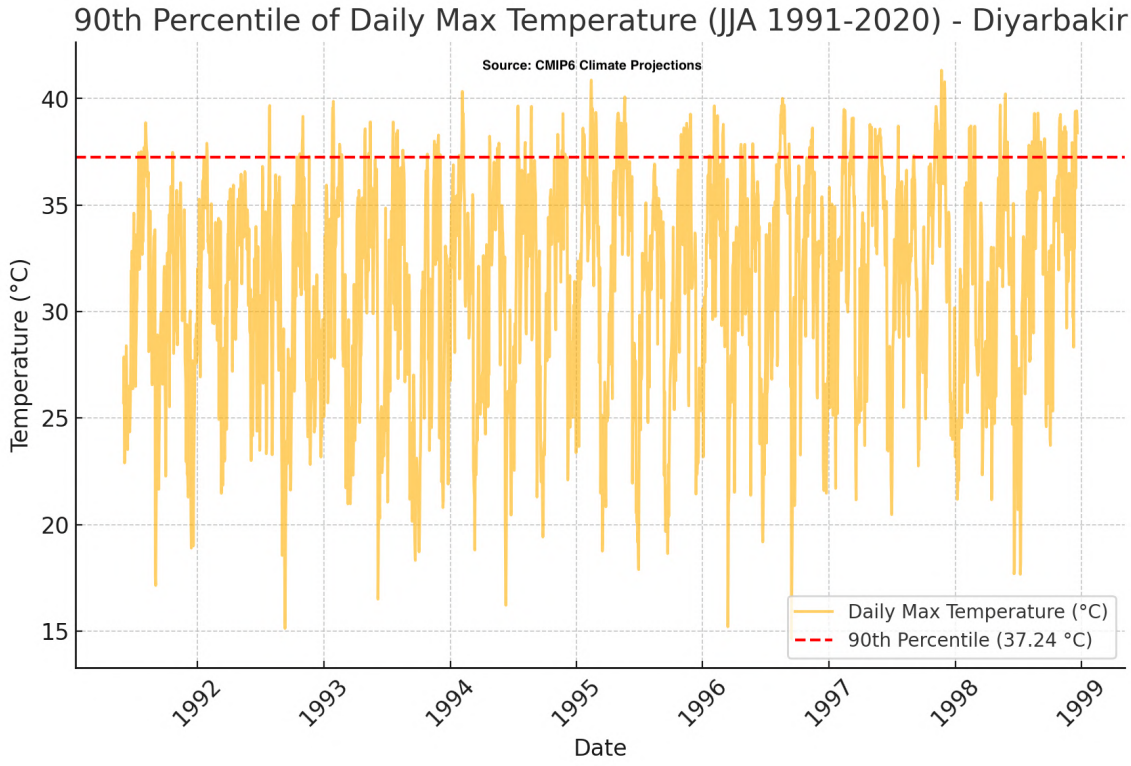

(a) 90th Percentile Threshold (1991–2020) – Diyarbakır

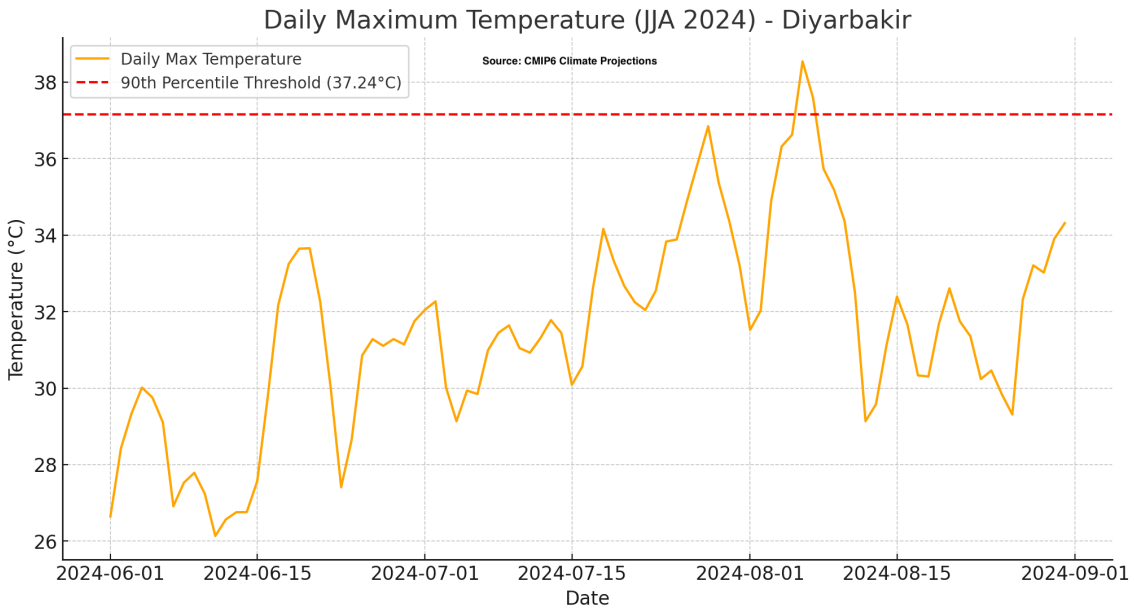

(b) Daily Max Temperatures – Summer 2024

Figure 3.4: Diyarbakır: Threshold validation and 2024 summer temperature comparison

Diyarbakır For Diyarbakr, the 90th percentile threshold was calculated at 37.24 ° C (panel a). During summer 2024, this threshold was frequently exceeded (panel b), especially in July. These hot days were used to validate extreme heat conditions and provided a temporal reference for acquiring Landsat imagery used in thermal mapping of the city.

These thresholds were then used to flag hot days in 2024 (see Section 3.3). Any day that exceeded the respective threshold was classified as an extreme heat day. These thresholds also served as input parameters for satellite image selection, ensuring that Landsat 8 and 9 imagery corresponded to thermally significant dates for LST analysis. The city-specific thresholds also offer a baseline for temporal comparison. For example, future climate scenarios can use these benchmarks to detect shifts in temperature distribution and the expansion of heat extremes. In summary, the 90th percentile method provides a robust location-specific metric to define heatwaves, integrating long-term climate behavior with short-term monitoring and remote sensing workflows. For example, in Erbil, the calculated 90th percentile threshold for summer maximum temperatures was 39.75°C. During the summer of 2024, multiple days in July and August exceeded this value, triggering classification as extreme heat events. Satellite imagery from August 6 and 10 was selected based on these exceedances and used to extract LST, which revealed thermal hotspots above 62°C in semi-developed areas near the city's periphery.

3.2 Urban Heat Island analyses

This section presents a detailed examination of the spatial distribution of LST during the summer of 2024 in the selected cities of Erbil, Diyarbakır, Urmia, and Kobani. The objective is to assess the UHI phenomenon and the variability in surface heat intensity across different land cover types. The analysis is based on satellite-derived thermal imagery corresponding to extreme heat days, which were identified using the 90th percentile threshold method derived from historical maximum air temperature records (1991–2020).

LST data were extracted from the thermal infrared (TIR) Band 10 of Landsat 8 and Landsat 9, using Level-2 Surface Temperature products available through the USGS Earth Explorer platform. These datasets are atmospherically corrected and emissivity-adjusted, offering reliable and standardized temperature outputs at a spatial resolution of 30 meters. The thermal images selected for each city correspond to specific dates in August 2024 when the daily maximum air temperature exceeded the computed 90th percentile threshold. This ensures that the remote sensing analysis is anchored in climatologically significant events, enhancing the robustness of the findings. All spatial analyses were conducted using QGIS software. The raw raster data were first clipped to 20 km buffer zones centered on each urban core to isolate the thermal characteristics of both built-up areas and surrounding peri-urban or rural zones.

Diyarbakır

The LST map of Diyarbakır reveals a classic urban heat island pattern. Higher surface temperatures are concentrated within the built-up urban core, with temperatures exceeding 56 °C in some locations. Peripheral areas exhibit moderately lower values, indicating vegetative or agricultural land uses that contribute to localized cooling. Spatial contrast highlights the role of surface type in influencing heat absorption and retention.

Figure 3.5: Location of Diyarbakır in the Kurdistan Region.

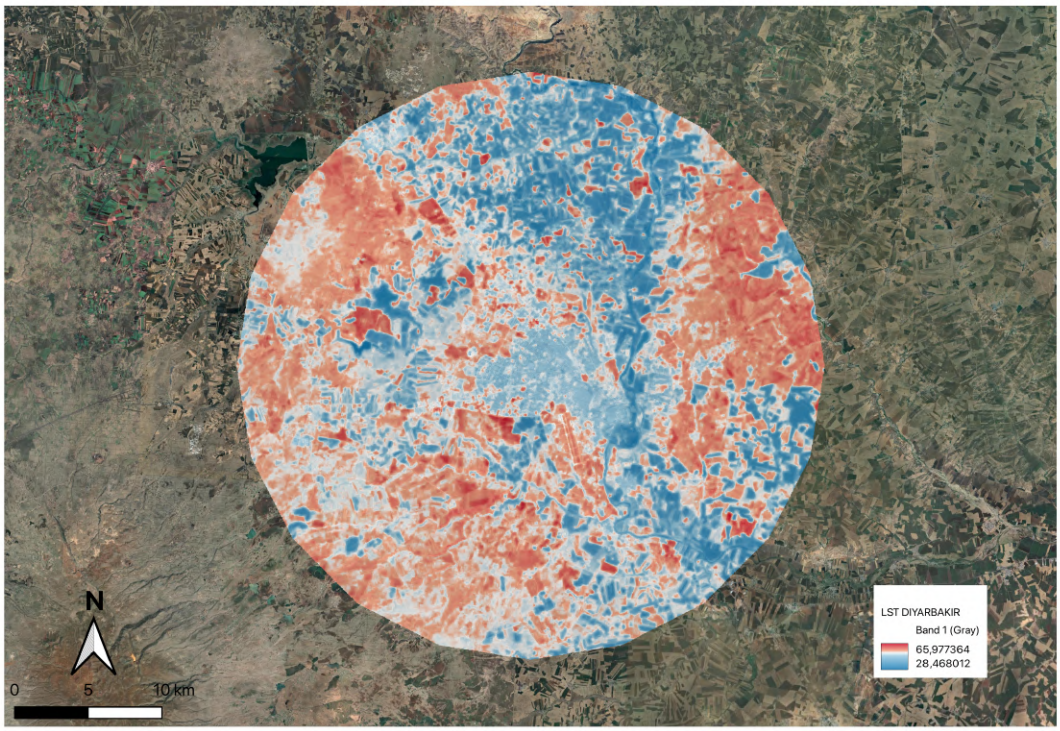

(a) Diyarbakır – 20 km buffer

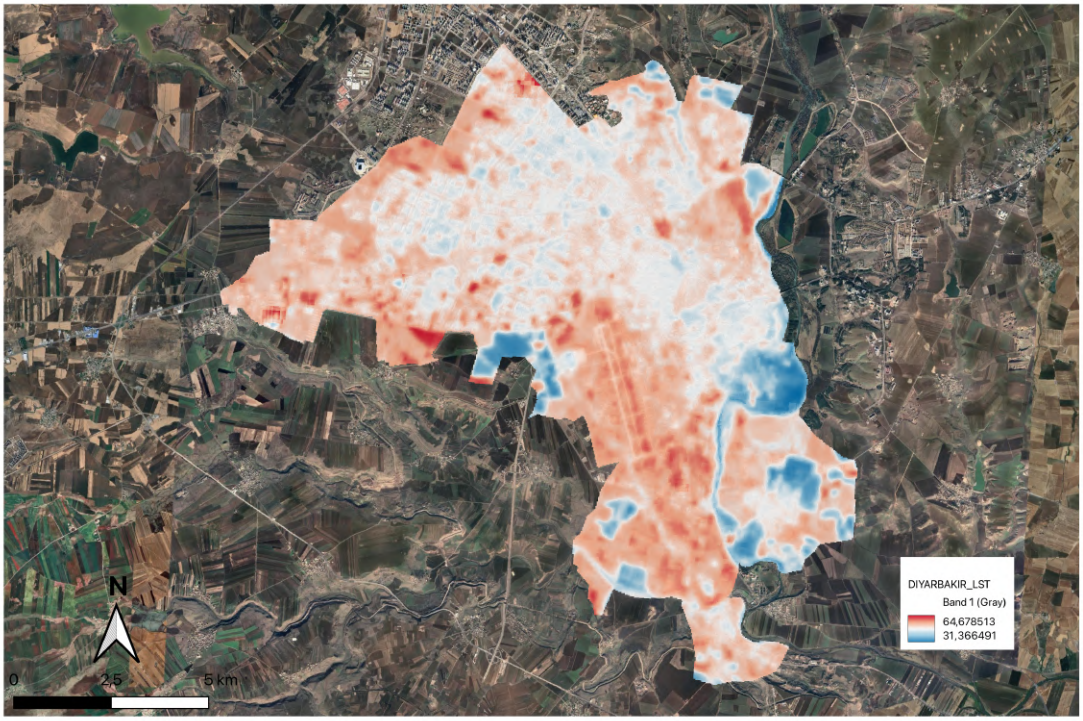

(b) Diyarbakır – municipal extent

Figure 3.6: Land Surface Temperature in Diyarbakır (August 2024).

Diyarbakır

Diyarbakr experienced heat events on 6 and 7 August, exceeding the 90th percentile threshold of 40.12, ° C. The highest surface temperature, 64.6, ° C, was recorded on the urban-agricultural fringe, where a band of newly constructed residential units borders expansive cultivated fields. The lack of tree cover and exposed soil, combined with the retention of heat from nearby infrastructure, contributed to a strong localized urban–rural heat gradient, even outside of the core urban area.

Figure 3.7: Landsat 8 satellite image of Diyarbakır's hottest urban zone, where land surface temperature reached 64.6°C (August 2024).

Erbil

Erbil's land surface temperature (LST) distribution during the 2024 summer heatwave exhibits a well-defined urban heat island (UHI) centered in the southern and southeastern districts of the city. The highest recorded surface temperature reached approximately 62.4 °C, concentrated in semi-developed or barren plots near major road networks. Surrounding built-up zones commonly ranged between 54 °C and 56 °C, especially in densely constructed sectors. Cooler areas, shown in light blue to blue on the LST map, are visible on the city's northwestern and peripheral edges, where urban density decreases and more agricultural or undeveloped land persists. These thermal patterns closely correspond to land cover distributions, with the hottest zones aligning with impervious, low-vegetation surfaces in the city's core.

Figure 3.8: Location of Erbil in the Kurdistan Region.

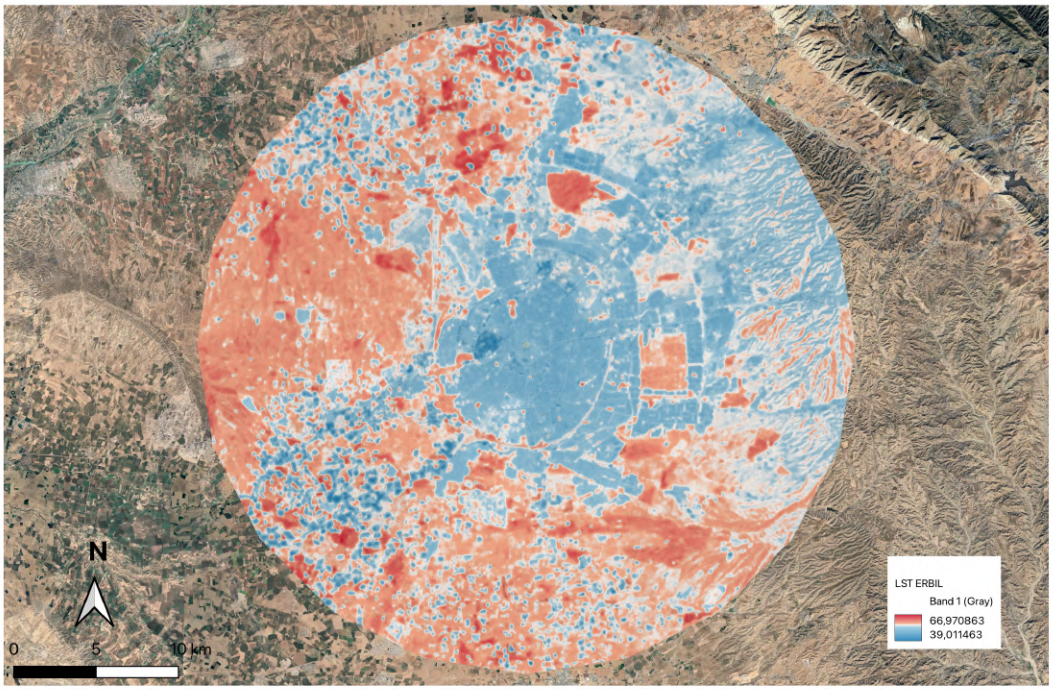

(a) Erbil – 20 km buffer

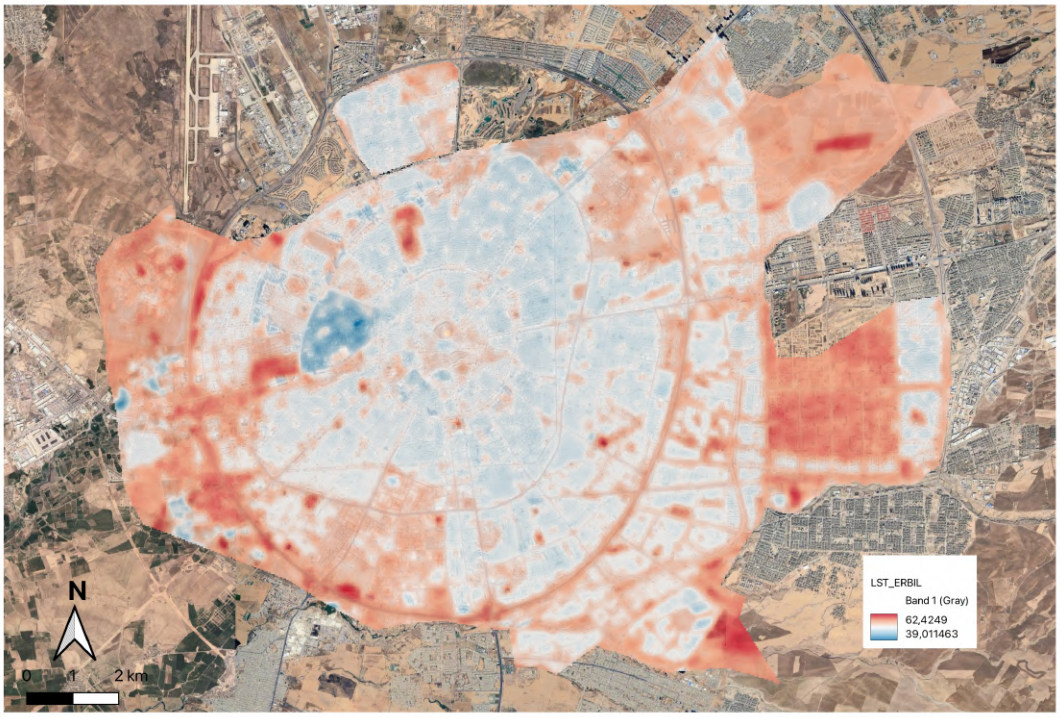

(b) Erbil – municipal extent

Figure 3.9: Land Surface Temperature in Erbil (August 2024).

Erbil

The hottest point, 62.4 °C, was located near a major highway junction on a bare, undeveloped tract, bordered by semi-urban plots and infrastructure corridors. The combination of asphalt surfaces, lack of vegetation, and urban expansion edge effects likely contributed to this extreme thermal hotspot.

Figure 3.10: Landsat 8 and 9 satellite image of Erbil's hottest urban zone, where land surface temperature reached 62.4°C (August 2024).

Kobani

LST mapping in Kobani shows a less distinct UHI but reveals elevated surface temperatures in abandoned or damaged areas, particularly on August 6. The thermal peak of 56.1 °C occurs over barren urban land, with minimal vegetation. Although Kobani's built-up footprint is smaller, the lack of green cover and structural deterioration contribute to intensified heat exposure.

Figure 3.11: Location of Kobani in the Kurdistan Region.

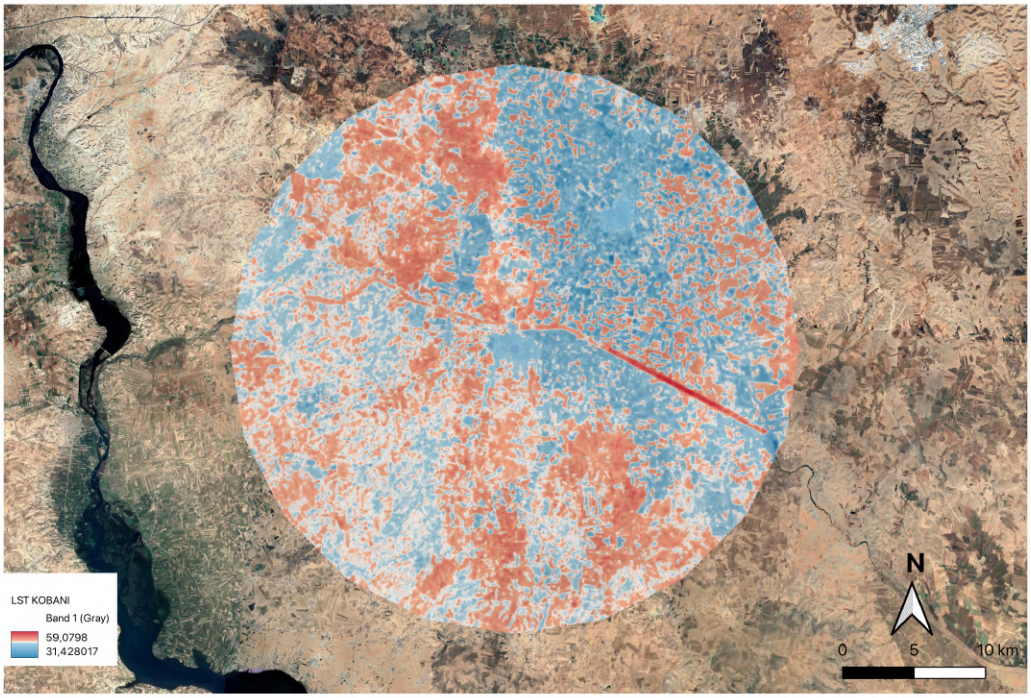

(a) Kobani – 20 km buffer

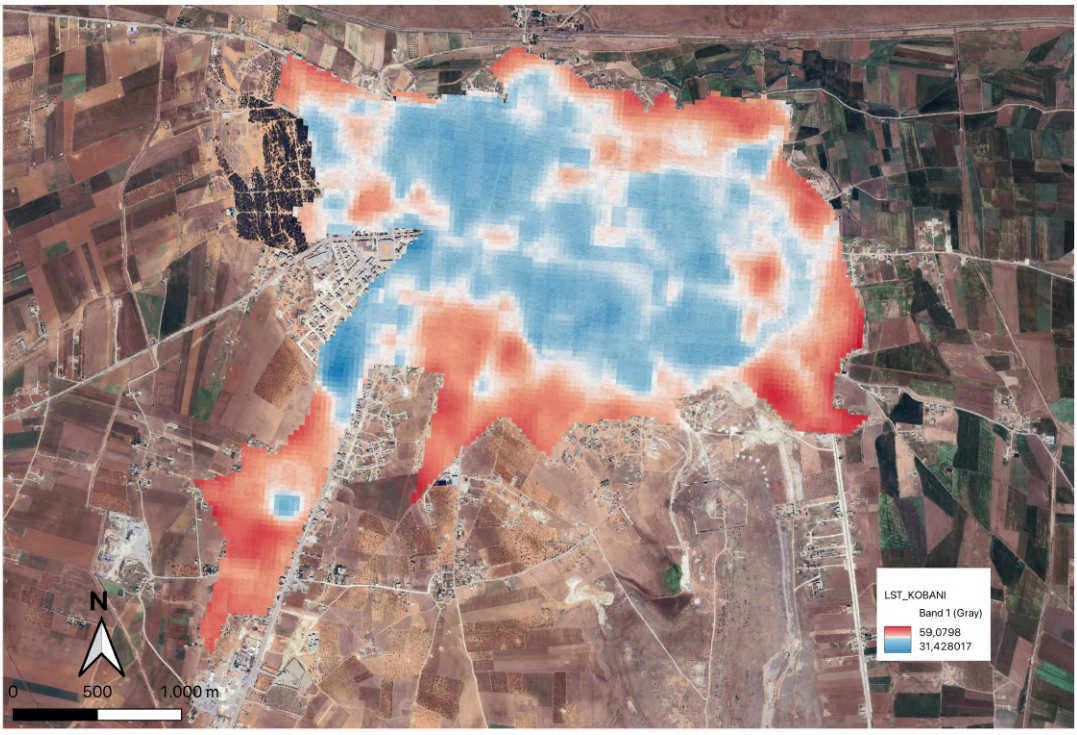

(b) Kobani – municipal extent

Figure 3.12: Land Surface Temperature in Kobani (August 2024).

Kobani

Kobani recorded a single heat wave event on 6 August, with air temperatures exceeding the city threshold of 39.45, ° C. The LST map highlighted a surface hotspot of 56.1 ° C within partially damaged or abandoned urban blocks. These zones, marked by barren land and degraded infrastructure, lack tree cover and moisture retention. This thermal profile underscores the vulnerability of post-conflict urban environments to extreme heat exposure.

Figure 3.13: Landsat 9 satellite image of Kobani's hottest urban zone, where land surface temperature reached 56.1°C (August 2024).

Urmia

Urmia exhibits a fragmented LST pattern, reflecting the city's varied topography and heterogeneous land cover. The highest surface temperatures, peaking at approximately 52.2 °C, are concentrated in the southwestern and southeastern fringes of the city, particularly in areas dominated by bare soil and minimal vegetation. In contrast, the central urban area remains comparatively cooler, likely due to irrigated green spaces, tree cover, and higher elevation. The LST map clearly shows a stark thermal gradient between cooler vegetated cores and the exposed, peripheral zones. This spatial variability is shaped by the transition between mountainous terrain, urban settlements, and open dry lands, underscoring the critical role of land cover and elevation in local heat dynamics.

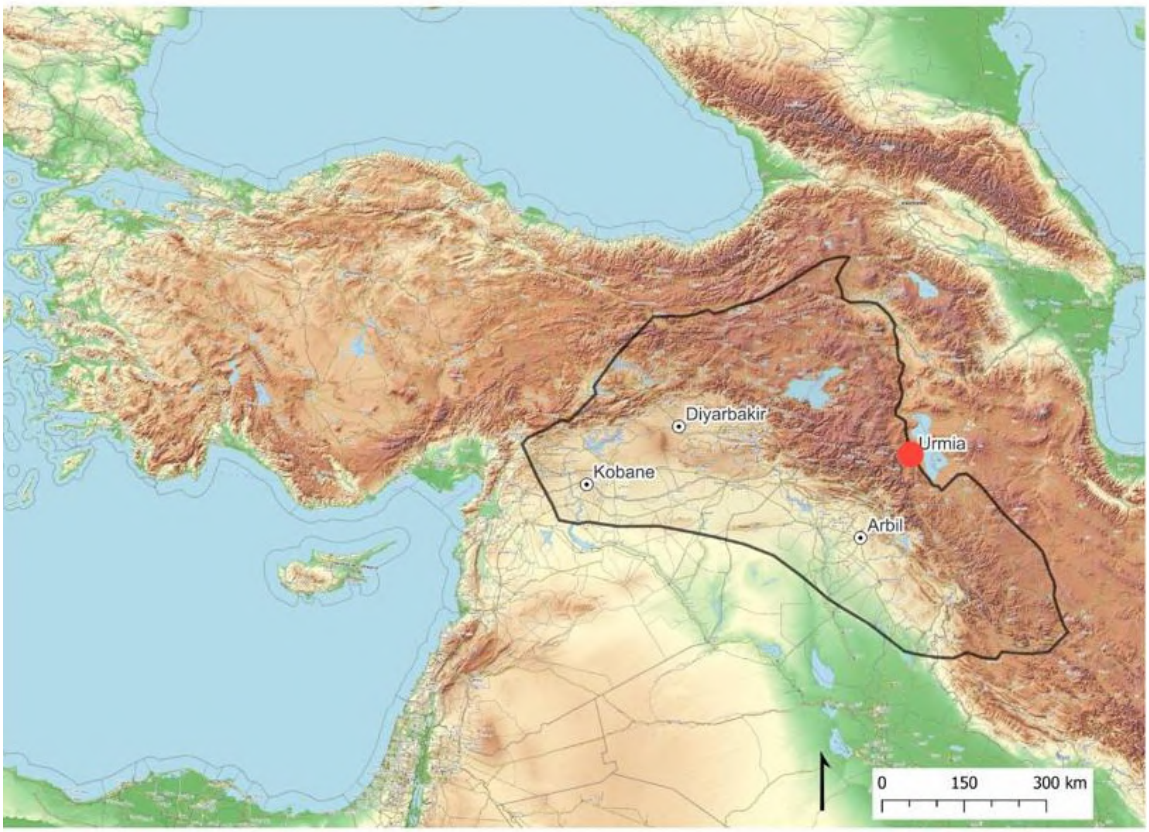

Figure 3.14: Location of Urmia in the Kurdistan Region.

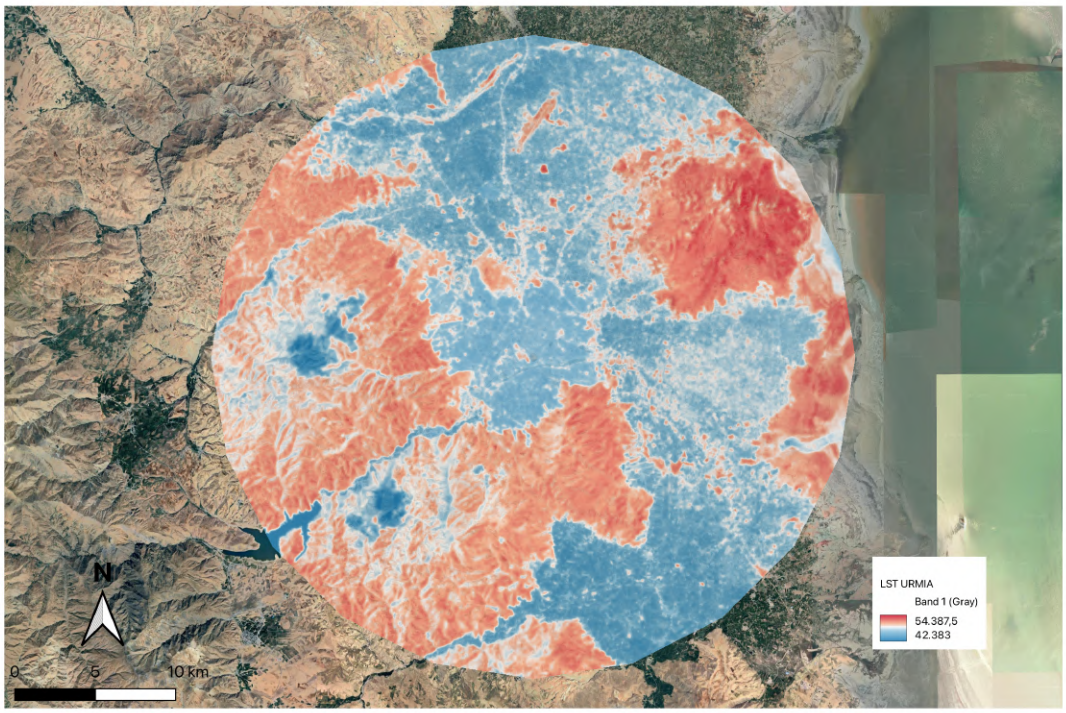

(a) Urmia – 20 km buffer

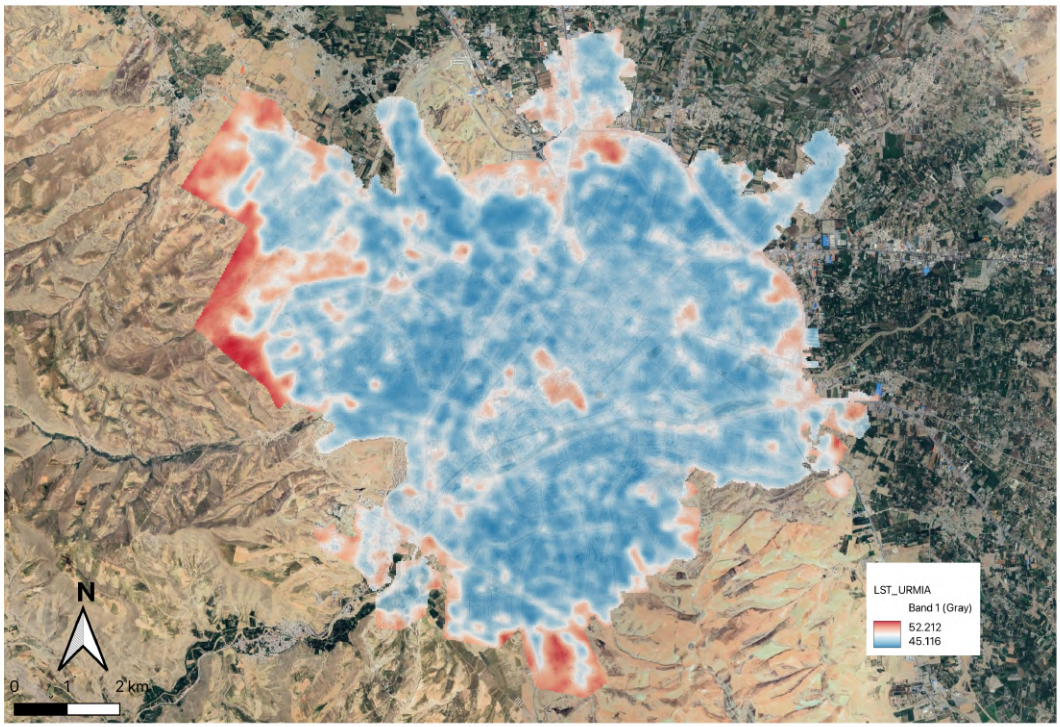

(b) Urmia – municipal extent

Figure 3.15: Land Surface Temperature in Urmia (August 2024).

Urmia

Urmia experienced an extended series of extreme heat days between July 29 and August 8, with the highest LST of 52.2 °C recorded in a dry, largely undeveloped plateau on the city's periphery. The zone is dominated by bare land and minimal land use activity, with scattered low-rise buildings and visible erosion. These conditions enhance solar absorption and inhibit cooling, particularly in the absence of vegetation and water bodies.

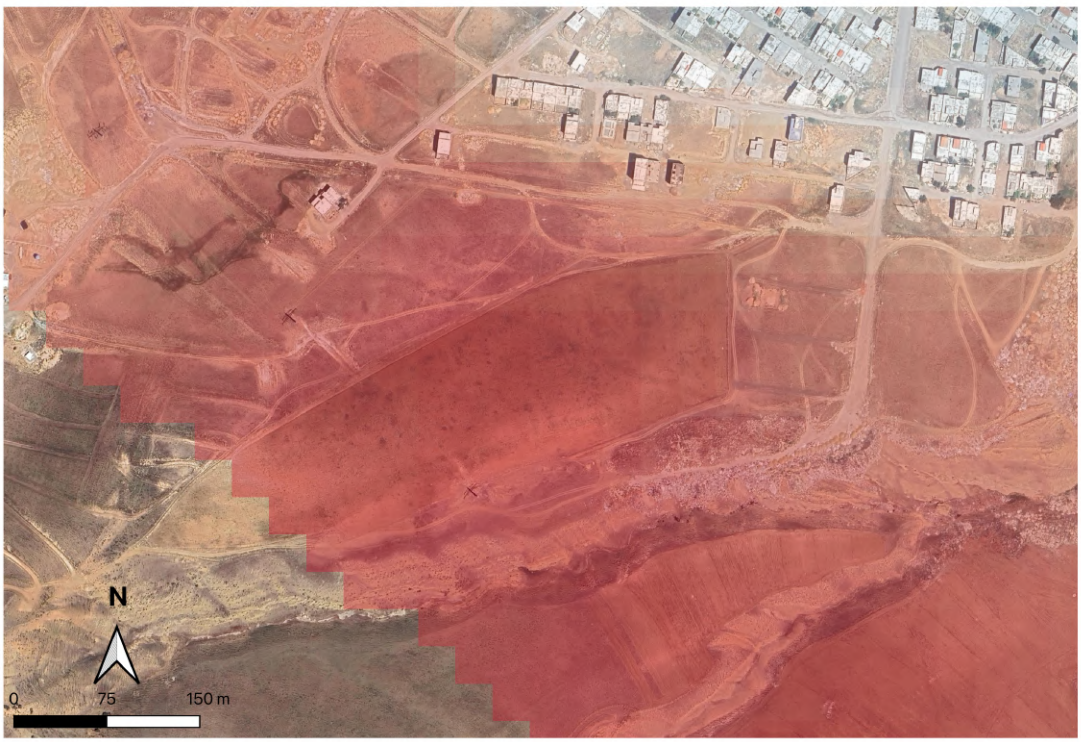

Figure 3.16: Landsat 8 and 9 satellite image of Urmia's hottest urban zone, where land surface temperature reached 52.2°C (August 2024).

Comparative analyses among the four study cases

This section compares the spatial distribution of urban heat exposure in the four case study cities—Erbil, Diyarbakır, Kobani, and Urmia—based on the Land Surface Temperature (LST) recovered during extreme heat days in August 2024. The comparative framework highlights how physical geography, urban morphology, and land use conditions shape thermal patterns and vulnerability in each location.

Among the cities studied, Diyarbakır and Erbil exhibited the highest surface heat intensity, with LST values exceeding 64.6°C and 62.4°C, respectively. These extreme values were strongly associated with dense built-up zones, characterized by high concentrations of impervious surfaces such as asphalt roads, concrete structures, and rooftop materials with low albedo. Both cities demonstrated well-defined Urban Heat Island (UHI) signatures, particularly in urban expansion areas where the absence of established green infrastructure exacerbated thermal retention. The spatial clustering of thermal hotspots in these urban cores underscores the amplifying effect of unregulated urban sprawl and the lack of vegetative buffers. These hot zones were concentrated in compact, densely developed areas with limited vegetation and high surface imperviousness, amplifying heat retention, especially in peripheral districts under active development.

In contrast, Urmia presented a more heterogeneous thermal landscape. Although subject to frequent heatwave conditions, the city's thermal hotspots were less intense and more fragmented. This is likely due to its elevation, surrounding topography, and integration of agricultural and vegetated zones, which buffer urban temperatures. While heat extremes were observed—reaching up to 52.2°C in the southwestern dry plateaus—cooler patches persisted within the city, especially in zones with irrigated cropland, tree cover, and varied elevation. Urmia's LST values reflect the protective effects of green infrastructure and the diversity of land cover. The fractured nature of Urmia's urban form and the presence of green patches provided partial thermal relief, suggesting a degree of climatic resilience, though this may be threatened by ongoing land degradation and water scarcity.

Kobani, although the least urbanized of the four, showed high LST values (56.1°C) in exposed, degraded areas. These zones, often located on the urban periphery or in post-conflict landscapes, lack both vegetation and surface development. Surface temperatures peaked particularly in abandoned or damaged urban areas consisting of exposed soil, rubble, and minimal vegetation, where the absence of shading and surface moisture significantly elevated local LST. This suggests that urban abandonment and soil degradation can produce heat risks comparable to those in dense cities. Post-conflict reconstruction gaps and infrastructural damage appear to play a critical role in the formation of these localized heat pockets. Unlike the compact UHI of Erbil or Diyarbakır, Kobani's thermal hotspots were more fragmented but no less severe,

indicating that vulnerability to heat is not solely a function of urban density but also of land condition and post-crisis land management.

Across all four cities, a clear pattern emerged: land use, vegetative cover, and urban morphology are key variables in determining the spatial distribution and intensity of heatwaves. Built-up and impervious areas consistently aligned with thermal maxima, while cropland, shrubland, and tree-covered zones contributed to lower surface temperatures. The presence or absence of water bodies, green belts, and urban vegetation further differentiated the thermal profiles. Cities with integrated ecological features displayed more fragmented and resilient heat patterns, while those lacking such infrastructure faced concentrated and extreme thermal stress. In general, the comparative results emphasize that extreme surface temperatures are not only a function of urban density but also of land condition, vegetation, and infrastructure quality.

These comparative findings highlight the need for differentiated urban planning strategies. In dense cities like Diyarbakır and Erbil, green infrastructure retrofitting and land use zoning are essential for reducing heat exposure. In environmentally sensitive or post-conflict settings like Kobani and Urmia, efforts should prioritize ecological restoration, land rehabilitation, and adaptive reuse of abandoned urban plots. The evidence strongly supports the integration of spatial heat analysis into climate adaptation policies across the Kurdistan region, where geopolitical and environmental fragility amplify the risks associated with extreme heat.

3.3 Land Cover Composition

Building on the methodology described in Section 2.1.3, this section presents the spatial distribution of land cover types in the municipal areas and surrounding 20 km buffer zones of the four case study cities: Erbil, Diyarbakir, Kobani, and Urmia. Land cover is a key factor in understanding how different surfaces interact with solar radiation and influence land surface temperature (LST). Vegetated areas such as croplands, grasslands, and tree cover typically support evapotranspiration and provide cooling, whereas built-up and bare surfaces absorb and retain heat, contributing to elevated urban temperatures. Analyzing land cover distributions in both core urban and peri-urban regions provides insight into the ecological and structural landscape surrounding each city. This information is essential for interpreting patterns of heat exposure, detecting urban heat island effects, and identifying areas most vulnerable to climate extremes.

3.4 Land use and land cover analyses

3.4.1 Diyarbakir

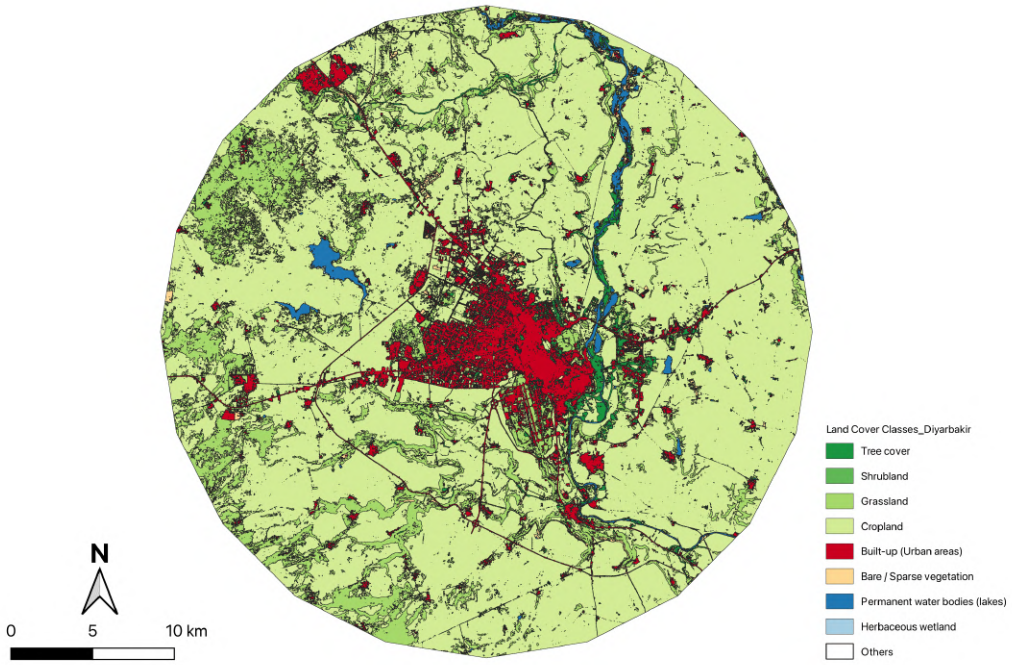

Figure 3.17: Land cover classification for Diyarbakir within 20 km buffer zone.

In Diyarbakir, the buffer zone is overwhelmingly dominated by *cropland* (85.1%), reflecting the city's strong agricultural interface. *Built-up areas* occupy only 6.5%, while *grassland* (6.1%) and minimal *tree cover* (1.1%) account for the remaining distribution. This land structure aligns with Diyarbakir's identity as a city embedded within a broader farming region. However, the scarcity of tree cover and lack of water bodies suggest that *evapotranspiration* and cooling potential remain limited outside the urban core, potentially contributing to high surface heat in surrounding croplands during drought periods.

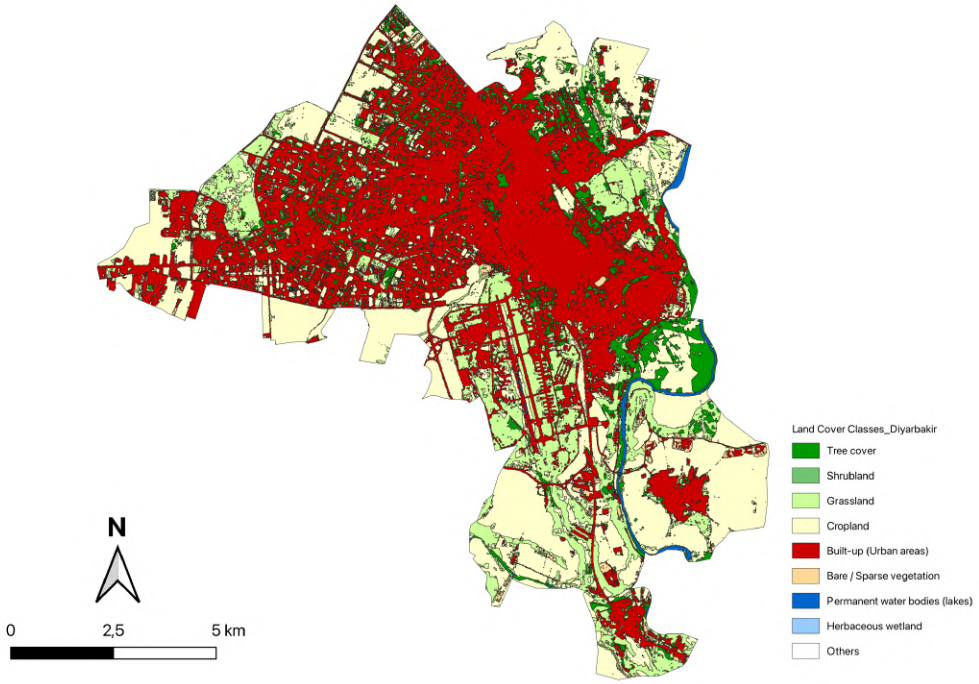

Figure 3.18: Land cover classification within Diyarbakir municipal boundary.

In contrast, Diyarbakır presents an urban-dominated land cover profile. *Built-up areas* constitute 85% of the municipal area, while *cropland* accounts for only 6.5% and *grassland* for 7.5%. Minor contributions come from *tree cover* (2.3%), *bare land* (0.6%), and *water* (0.4%), with *wetlands* and *shrubland* being negligible. The spatial dominance of impervious surfaces confirms the intense urban character of the city, despite some presence of vegetation and agricultural land. This pattern contributes to higher surface heat accumulation and underscores Diyarbakır's vulnerability to extreme heat events and drought-related thermal stress.

3.4.2 Erbil

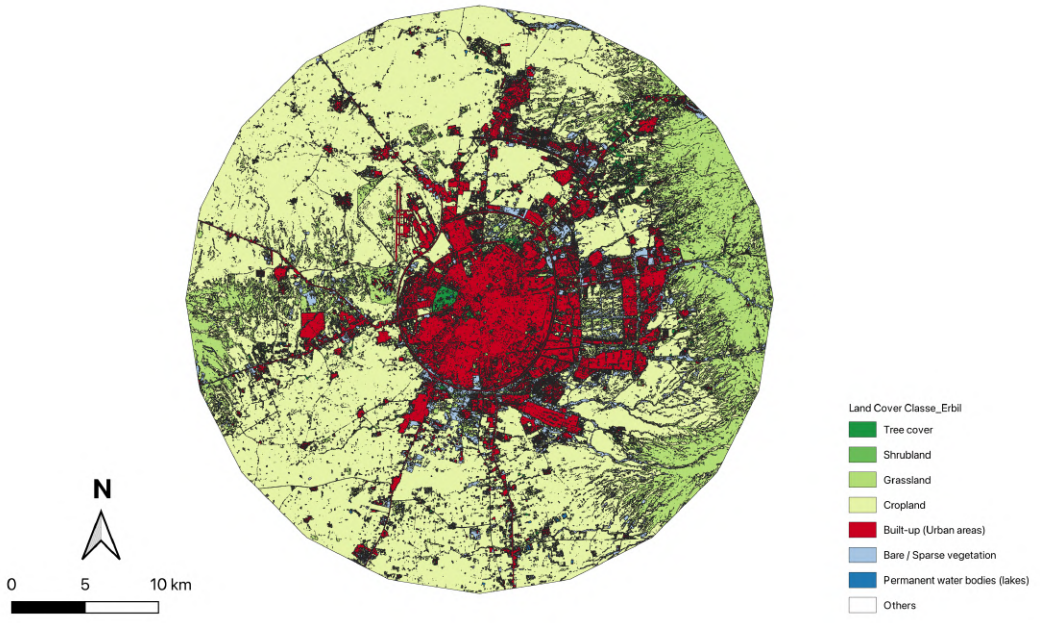

Figure 3.19: Land cover classification for Erbil within 20 km buffer zone.

In the Erbil buffer zone, *cropland* accounts for the largest land class at 47.6%, followed by *grassland* (29.8%) and *built-up areas* (13.9%). *Tree cover* makes up only 3.7%, while *bare/sparse vegetation* and *shrubland* collectively contribute less than 5%. This composition suggests a semi-urban fringe with dominant agricultural use, interspersed with pockets of urban expansion. Despite the city's highly urbanized municipal core, the surrounding landscape shows relatively high green coverage, offering moderate buffering against heat buildup, though insufficient vegetative shading and minimal water presence may still exacerbate heat risks.

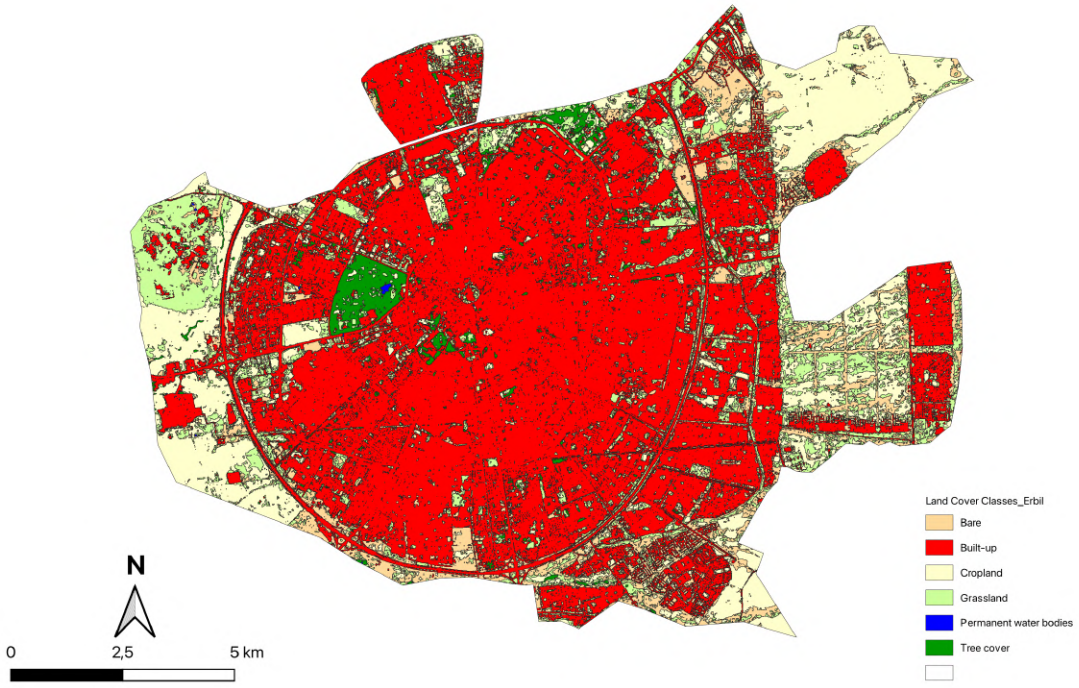

Figure 3.20: Land cover classification within Erbil municipal boundary.

Erbil shows the most pronounced urban concentration among the three cities, with *built-up land* covering 92.8% of its municipal area. This leaves minimal room for *grassland* (2.5%), *tree cover* (1.7%), *bare soil* (2.1%), and *cropland* (0.9%). The absence of significant *water bodies* and natural vegetation intensifies its surface heat retention, making it particularly susceptible to extreme temperature events. The high density of impervious surfaces combined with limited vegetative cover positions Erbil as a key hotspot for studying urban thermal anomalies and planning mitigation through green infrastructure.

3.4.3 Kobani

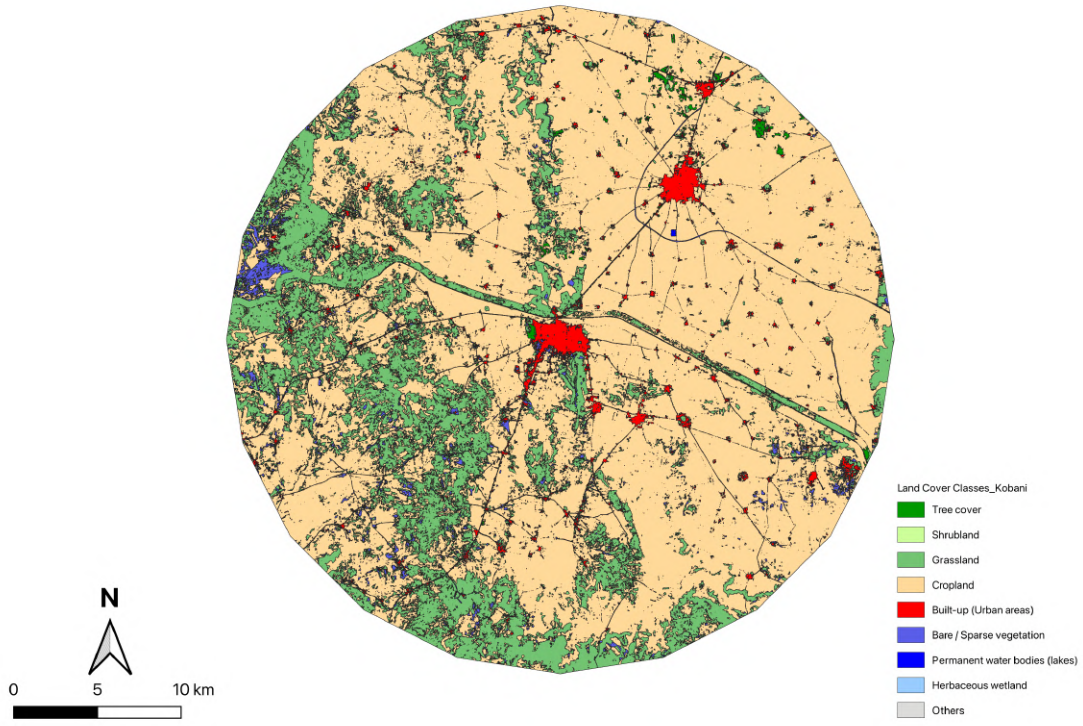

Figure 3.21: Land cover classification for Kobani within 20 km buffer zone.

The analysis reveals a landscape predominantly composed of bare or sparsely vegetated areas (54.6%), followed by shrubland (8.4%), and smaller shares of grassland, cropland, and built-up land. This composition highlights the peri-urban and degraded rural nature of the surrounding environment. Despite some presence of vegetation, the high percentage of exposed and sparsely vegetated surfaces may intensify surface heat retention, especially during extreme climate conditions. The relatively limited built-up area suggests that urban heat may be less concentrated compared to denser cities, but localized heating in barren or undeveloped zones remains a substantial concern.

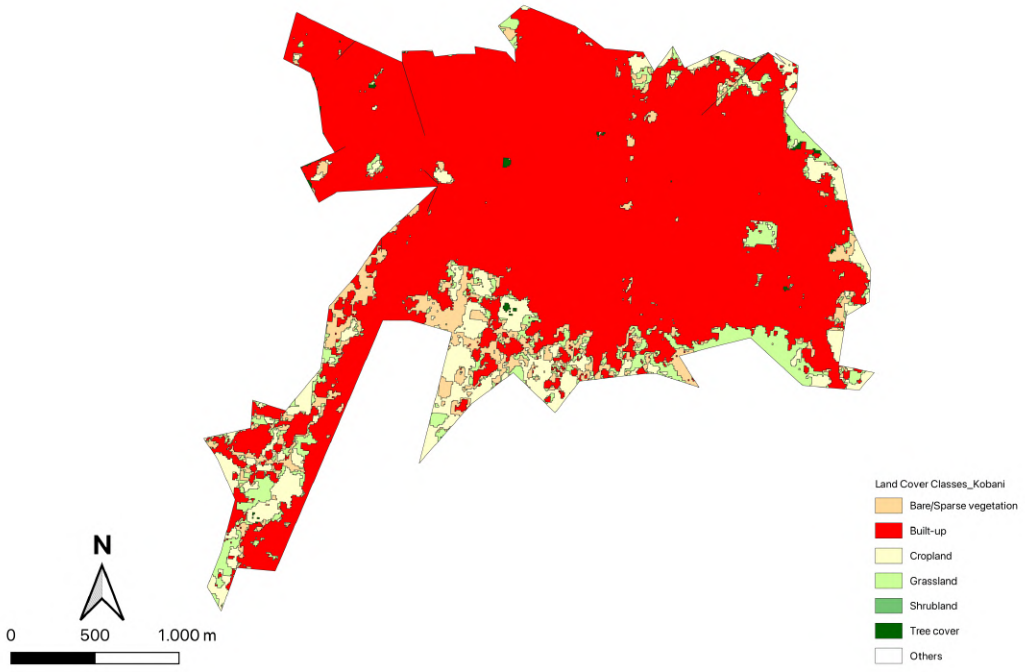

Figure 3.22: Land cover classification within Kobani municipal boundary.

Within this defined extent, land cover classification shows that built-up areas dominate the urban landscape, accounting for 86.0% of the surface. This is followed by grassland (5.5%), bare or sparsely vegetated land (4.1%), and cropland (4.0%), while other land cover types make up smaller proportions. This configuration reflects the highly urbanized yet fragmented nature of Kobani's municipal extent, where post-conflict development and infrastructure gaps have created thermally exposed zones. These barren or built-up surfaces strongly correspond with thermal hotspots identified in the LST imagery for summer 2024, where surface temperatures peaked at 56.1C. The findings underscore the critical role of vegetation in mitigating heat and highlight the urgent need to reintegrate green cover and ecological infrastructure in the city's ongoing redevelopment process.

3.4.4 Urmia

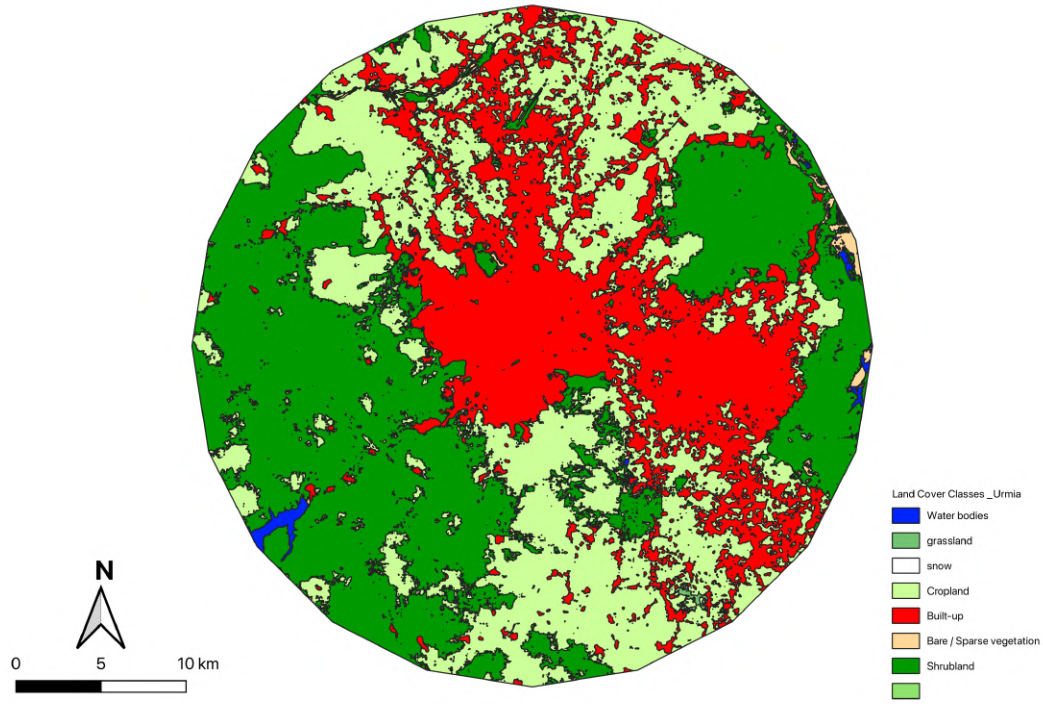

Figure 3.23: Land cover classification for Urmia within 20 km buffer zone.

In contrast, Urmia's buffer zone displays greater ecological diversity. cropland (30.3%) and shrubland (24.0%) are dominant. Built-up areas account for 18.2%, primarily concentrated in the city center. Although permanent water bodies (5.0%) occupy a relatively small share, the extensive presence of natural vegetation and agricultural land enhances the region's resilience to heat extremes. This ecological composition promotes *evapotranspiration and surface cooling*, offering protective effects compared to more urbanized environments.

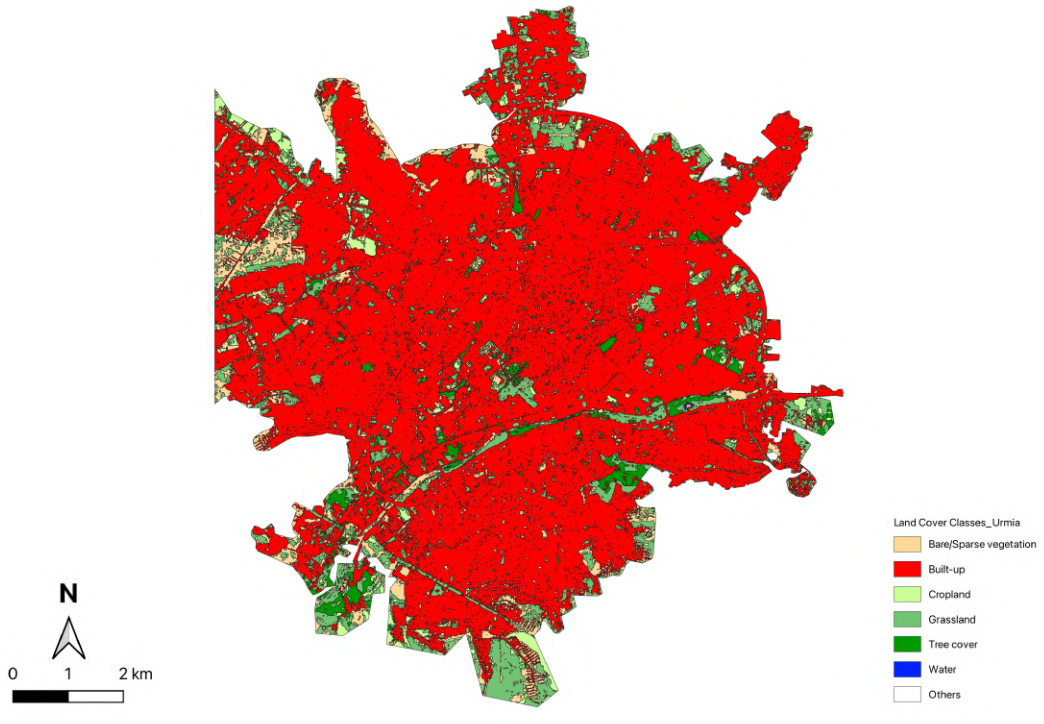

Figure 3.24: Land cover classification within Urmia municipal boundary.

In Urmia, the dominant land cover class is *built-up areas*, accounting for 75.6% of the municipal extent. This is followed by *grassland* (10.4%), *bare/sparse vegetation* (9.2%), *tree cover* (2.5%), and *cropland* (2.3%), with *water bodies* effectively absent (0.0%). The spatial pattern suggests a dense urban core surrounded by fragmented patches of natural and agricultural land, contributing to the effects of the urban heat island (UHI) and reducing the permeability of the surface.

Across the four cities in the case study, a comparative analysis of land cover within both the municipal boundaries and surrounding 20 km buffer zones reveals important spatial contrasts that help explain differences in surface heat intensity. Diyarbakır and Erbil demonstrate the most urbanized municipal profiles, with built-up areas accounting for 85.0% and 92.8% of their respective city extents. These dense urban cores are characterized by low vegetation coverage and a dominance of impervious surfaces, such as roads and rooftops, which correspond to the highest land surface temperatures (LST) recorded in the study: 64.6 ° C in Diyarbakr and 62.4 ° C in Erbil. In both cases, the surrounding buffer zones are also dominated by altered landscapes by humans. The Diyarbakr buffer area, for example, consists of 85. 1% cropland and only 1. 1% tree cover, offering limited ecological cooling. Erbil's buffer is somewhat more mixed, with 47.6% cropland and 29.8% grassland, yet it still lacks significant tree cover or water bodies that could regulate local microclimates.

In contrast, Kobani and Urmia have more fragmented and ecologically diverse landscapes. Kobani's municipal area, although built-up by 86.0%, still includes a mix of cropland (4.0%), grassland (5.5%), tree cover (0.4%), and bare land (4.1%)—a distribution that contrasts with the even more densely urbanized cities. Its buffer zone is dominated by bare or sparsely vegetated land (54.6%), reflecting a post-conflict context with widespread land degradation and minimal reforestation. These surface conditions contribute to localized heat anomalies, with LST peaks reaching 56.1 °C, even in the absence of dense urbanization. Urmia, meanwhile, combines a high built-up ratio in its municipal area (75.6%) with the most ecologically varied buffer zone of the four cities. Its surrounding 20 km area includes 30.3% cropland and 24.0% shrubland, along with a small presence of water bodies (5.0%). These types of land cover contribute to thermal fragmentation and moderate LST values, with the highest surface temperature observed at 52.2 °C.

In general, the comparative profiles of municipal and buffer zones in these cities underscore the critical role of surrounding land cover in shaping urban thermal dynamics. Built-up areas alone do not fully determine heat exposure; instead, the combination of surface materials, vegetation availability, and broader ecological context governs the severity and distribution of urban heat. These findings highlight the need for integrative land use planning that addresses both city centers and peri-urban fringes to improve climate resilience in Kurdistan's urban regions.

4 Conclusions

This thesis explored the spatial patterns and climatic impacts of heatwaves and extreme temperature events in the Kurdistan region, focusing on four cities—Erbil, Diyarbakır, Kobani, and Urmia—selected for their geographic, political, and ecological diversity. By integrating long-term climate data from CMIP6 and ERA5 with satellite-derived Land Surface Temperature (LST) from Landsat 8 and 9, and combining this with high-resolution land cover information from the ESA WorldCover dataset, the study applied a robust geospatial and climatological approach to analyze how land use, urban morphology, and ecological degradation shape local thermal extremes.

The research established city-specific temperature thresholds based on the 90th percentile of historical daily maximum temperatures, which allowed for the identification of extreme heat days in the summer of 2024. These days were then used to select representative satellite imagery for spatial analysis. The results revealed alarming heat intensities, with Diyarbakır and Erbil recording the highest LST values, exceeding 64°C and 62°C respectively. These hotspots were strongly associated with densely built-up urban zones lacking vegetation and green infrastructure, underscoring the intensity of the Urban Heat Island (UHI) effect in rapidly expanding cities with unregulated development.

In contrast, Urmia demonstrated more spatially heterogeneous thermal patterns. Its ecological diversity, varying topography, and the presence of peri-urban vegetation appeared to buffer against extreme heat concentrations, although land degradation and the shrinking of Lake Urmia pose growing risks. Kobani, while less urbanized, exhibited severe heat pockets in abandoned or damaged zones, where the absence of tree cover and soil moisture amplified surface temperatures. This finding highlights that vulnerability to extreme heat is not only a function of urban density but also of post-conflict land degradation and infrastructural disrepair.

The relationship between land cover and thermal exposure emerged as a critical factor. Built-up and bare land areas consistently aligned with high LST zones, while vegetated surfaces such as croplands, grasslands, and tree-covered areas demonstrated cooling effects through evapotranspiration. Yet, the municipal extents of all four cities showed alarmingly low percent-

ages of natural vegetation and tree cover, reinforcing the urgent need for green infrastructure in climate adaptation strategies.

Overall, the integration of GIScience, satellite remote sensing, and climate modeling provided a powerful and scalable framework for assessing heat risk in the geopolitically fragmented and ecologically stressed context of Kurdistan. The findings not only advance scientific understanding of climate extremes in underrepresented regions but also deliver evidence-based insights for urban planners, environmental policymakers, and civil society actors. As climate change continues to escalate, cities in Kurdistan must prioritize ecological restoration, climate-resilient infrastructure, and equitable land use planning to reduce heat vulnerability and protect both human and environmental health.

Bibliography

[1] Hess, J. J., Saha, S., & Luber, G. (2023). Public health preparedness for extreme heat events. *Annual Review of Public Health, 44*, 301–321. https://doi.org/10.1146/annurev-publhealth-071421-025508

[2] World Meteorological Organization. (2022). *State of the Global Climate 2022*. https://wmo.int/publication-series/state-of-global-climate-2022

[3] Field, C. B., Barros, V. R., Stocker, T. F., & Qin, D. (Eds.). (2012). *Managing the risks of extreme events and disasters to advance climate change adaptation*. Cambridge University Press.
https://www.ipcc.

[4] Huang, C., Barnett, A. G., Wang, X., Vaneckova, P., FitzGerald, G., & Tong, S. (2011). Projecting future heat-related mortality under climate change scenarios: A systematic review. *Environmental Health Perspectives, 119*(12), 1681–1690. https://doi.org/10.1289/ehp.1103456

[5] Stone, B. Jr., Vargo, J., Habeeb, D., Hess, J. J., & Franzini, L. (2014). Managing climate change risks in cities: A framework for climate-resilient urban design. *Environmental Science & Policy, 44*, 75–85. https://doi.org/10.1016/j.envsci.2014.07.003

[6] Haines, A., Kovats, R. S., Campbell-Lendrum, D., & Corvalán, C. (2006). Climate change and human health: Impacts, vulnerability and public health. *The Lancet, 367*(9528), 2101–2109. https://doi.org/10.1016/S0140-6736(06)68933-2

[7] Council on Foreign Relations. (2014). *Kurdish population estimates*. https://www.cfr.org

[8] CityPopulation.de. (2025). *Diyarbakır, Erbil, Urmia population data*. https://www.citypopulation.de

[9] Beck, H. E., Zimmermann, N. E., McVicar, T. R., Vergopolan, N., Berg, A., & Wood, E. F. (2018). Present and future Köppen-Geiger climate classification maps at 1-km resolution. *Scientific Data, 5*, 180214. https://doi.org/10.1038/sdata.2018.214

[10] ESA WorldCover. (2021). *Land Cover Map – User Guide v2.0*. https://esa-worldcover.org

[11] USGS Earth Explorer. (2024). *Landsat 8 & 9 surface temperature datasets*. https://earthexplorer.usgs.gov/

[12] Australian Bureau of Meteorology. (n.d.). *Climate statistics: Percentile calculations explained*. Retrieved July 3, 2025, from http://www.bom.gov.au/climate/

[13] Rudaw Media Network. (2025). *Kurdistan farmers face heat and drought challenges*. https://www.rudaw.net

[14] Mohammad, A. T., Zare, M., & Karimian, A. (2025). Drought risk assessment in Iran's Kurdistan province. *Iranian Journal of Natural Hazards, 14*(2), 115–129.

[15] C2ES – Center for Climate and Energy Solutions. (2025a). *Climate impacts on water*. https://www.c2es.org/content/climate-impacts-on-water-resources/

[16] C2ES – Center for Climate and Energy Solutions. (2025). *Heatwaves and urban heat island effects*. https://www.c2es.org

[17] Elias Modern Press. (1946). *Ethnic map of Kurdistan* [Map]. Cairo, Egypt.

[18] O'Shea, M. T. (2004). *Trapped Between the Map and Reality: Geography and Perceptions of Kurdistan*. Routledge.

[19] KHRP – Kurdish Human Rights Project. (1995). *The Kurds: A Contemporary Overview*. London: Frank Cass.

[20] Rojava Information Center. (2023). *The Social Contract of North and East Syria*. https://rojavainformationcenter.com

[21] Naumann, G., & Formetta, G. (2020). Urban population exposure to heatwaves in Europe. *Nature Communications, 11*, 3681. https://doi.org/10.1038/s41467-020-17401-1

[22] Liu, H., & Zhang, Q. (2005). Assessment of urban heat island and mitigation strategies using remote sensing data. *Remote Sensing of Environment, 94*(3), 321–336. https://doi.org/10.1016/j.rse.2004.11.006

[23] USGS. (2024). *Landsat Collection 2 Level-2 Science Products Guide*. https://www.usgs.gov

[24] CityPopulation.de. (2016). *Urmia: Population statistics and maps*. https://www.citypopulation.de/en/iran/westazerbaijan/urmia/

[25] Kurdish Institute of Paris. (n.d.). *Kurdish dialects and regions*. Retrieved July 3, 2025, from https://www.institutkurde.org

[26] Kurdish Times. (1999). Social structure of the Kurds. *The Kurdish Times, 13*(2), 5–19.

[27] Copernicus Climate Change Service. (2024). *ERA5 and CMIP6 datasets*. https://cds.climate.copernicus.eu

[28] IPCC. (2021). *Sixth Assessment Report Summary for Policymakers*. https://www.ipcc.ch/report/ar6/syr/

[29] KRG – Kurdistan Regional Government. (2025). *About Erbil*. https://gov.krd/erbil/

[30] OpenStreetMap Contributors. (2024). *Kobani city layout*. https://www.openstreetmap.org

[31] QGIS Development Team. (2024). *QGIS: A free and open-source geographic information system*. https://qgis.org

[32] Open Geospatial Consortium. (2022). *Standards for geospatial data analysis*. https://www.ogc.org

[33] IPCC. (2014). *Climate Change 2014: Impacts, Adaptation, and Vulnerability*. Cambridge University Press.

[34] Rojava Information Center. (2023). *Ecological Charter of North and East Syria*. https://rojavainformationcenter.com/ecology

[35] Harvard University Map Collection. (1948). *Historic CIA map of Kurdistan*.

[36] McDowall, D. (2004). *A Modern History of the Kurds* (3rd ed.). I.B. Tauris.

[37] Stone, B., Vargo, J., & Habeeb, D. (2014). Urban form and heat: Strategies for mitigation. *Urban Climate, 10*, 197–214.

[38] Environmental Systems Research Institute (ESRI). (2022). *Shapefile format specification*. https://support.esri.com

[39] European Union Satellite Centre. (2021). *Sentinel-2 Land Cover data*. https://land.copernicus.eu

[40] GISGeography. (2023). *What is raster vs vector in GIS?* https://gisgeography.com

[41] IPCC. (2007). *Fourth Assessment Report: Climate Change 2007*. https://www.ipcc.ch

[42] Stone, B. (2012). *The City and the Coming Climate: Climate Change in the Places We Live*. Cambridge University Press.

[43] ArcGIS Online. (2023). *Urban heat risk mapping tools*. https://www.arcgis.com

[44] Haines, A., Kovats, R. S., et al. (2006). Public health adaptation to climate change: Lessons from past experiences. *The Lancet, 367*(9528), 101–108.

[45] Intergovernmental Panel on Climate Change (IPCC). (2021). *Climate Change 2021: The Physical Science Basis*. Contribution of Working Group I to the Sixth Assessment Report. https://www.ipcc.ch/report/ar6/wg1/

[46] World Meteorological Organization. (2023). *State of the Global Climate 2023*. https://public.wmo.int/en/our-mandate/climate/wmo-statement-state-of-global-climate

[47] Yang, X., et al. (2021). Response mechanism of plants to drought stress. *Horticulturae, 7*(3), 50. https://doi.org/10.3390/horticulturae7030050

[48] Wang, S., et al. (2021). Changes in carbon uptake associated with plant stress and climate extremes. *Urban Ecosystems*. https://doi.org/10.1007/s11252-021-01104-8

[49] Liu, X., Wang, F., Zhang, Y., Xu, L., & Zheng, Q. (2023). Impacts of vegetation loss on urban surface temperatures during extreme heat events. *Environmental Research Letters, 18*(4), 045001. https://doi.org/10.1088/1748-9326/acbef7

[50] Oke, T. R. (1973). City size and the urban heat island. *Atmospheric Environment, 7*(8), 769–779. https://doi.org/10.1016/0004-6981(73)90140-6

[51] The Kurdish Project. (n.d.). *Kurdistan map*. Retrieved July 3, 2025, from https://thekurdishproject.org/kurdistan-map/

[52] Kurdistan Regional Government. (n.d.). *Kurdistan Region overview*. Retrieved July 3, 2025, from https://gov.krd/english/

[53] World Bank. (2017). *The toll of war: The economic and social consequences of the conflict in Syria*. https://www.worldbank.org

[54] Valensi, C., Efron, S., & Noach, K. (2021). *A decade of war in Syria: Between climate change and political stability (INSS Insight No. 1449)*. https://www.inss.org.il/publication/syria-climate-change/

[55] Bounoua, L., Zhang, P., Imhoff, M. L., Wolfe, R. E., & Thome, K. J. (2015). Impact of urbanization on U.S. surface climate. *Environmental Research Letters, 10*(8), 084010. https://doi.org/10.1088/1748-9326/10/8/084010

[56] Kumar, D., & Shekhar, S. (2015). Urban heat island effect analysis using remote sensing and GIS: A case study of Delhi. *International Journal of Remote Sensing and GIS, 4*(1), 1–8.

[57] Akbari, H., & Rose, L. S. (2008). Urban surfaces and heat island mitigation potentials. *Lawrence Berkeley National Laboratory*. https://escholarship.org/uc/item/9pq8793d

[58] Stone, B., Hess, J. J., & Frumkin, H. (2010). Urban form and extreme heat events: Are sprawling cities more vulnerable to climate change than compact cities? *Environmental Health Perspectives, 118*(10), 1425–1428. https://doi.org/10.1289/ehp.0901879

[59] Sangiorgio, V., Ruggeri, D., & Murgante, B. (2020). Heatwave risk in cities: The role of urban morphology and design. *Sustainability, 12*(12), 5075. https://doi.org/10.3390/su12125075

[60] Mohajerani, A., Bakaric, J., & Jeffrey-Bailey, T. (2017). The urban heat island effect, its causes, and mitigation, with reference to the thermal properties of asphalt concrete. *Journal of Environmental Management, 197*, 522–538. https://doi.org/10.1016/j.jenvman.2017.03.095

[61] Yildiz, K. (2004). *The Kurds in Iraq: The past, present and future*. Pluto Press.

[62] Saeedpour, V. (1999). The Kurdish tribes and their traditions: A sociocultural perspective. *The Kurdish Times, 13*(2), 11–23.

[63] McDowall, D. (2004). The land of the Kurds. In *The Encyclopaedia of Kurdistan*. Kurdish Institute of Paris. Retrieved July 3, 2025, from http://www.kurdistanica.com/english/geography/geography-frame.html

[64] Kumar, D., & Shekhar, S. (2015). Statistical analysis of land surface temperature–vegetation indexes relationship through thermal remote sensing. *Ecotoxicology and Environmental Safety, 121*, 39–44. https://doi.org/10.1016/J.ECOENV.2015.07.004

[65] Kim, S. W., & Brown, R. D. (2021). Urban heat island (UHI) variations within a city boundary: A systematic literature review. *Renewable and Sustainable Energy Reviews, 148*, 111256. https://doi.org/10.1016/J.RSER.2021.111256

[66] Weng, Q. (2009). Thermal infrared remote sensing for urban climate and environmental studies: Methods, applications, and trends. *ISPRS Journal of Photogrammetry and Remote Sensing, 64*(4), 335–344. https://doi.org/10.1016/j.isprsjprs.2009.03.007

[67] Zanaga, D., Van De Kerchove, R., Xu, P., et al. (2022). *ESA WorldCover 10m 2021 v200 Product User Manual*. European Space Agency. https://doi.org/10.5281/zenodo.7254221

[68] Lupia, A. (2010). Environmental monitoring through GIS and remote sensing contributions.

[69] Intergovernmental Panel on Climate Change. (2018). *Global warming of 1.5°C: An IPCC special report*. https://www.ipcc.ch/sr15/

[70] Perkins, S. E., & Alexander, L. V. (2013). On the measurement of heatwaves. *Journal of Climate, 26*(13), 4500–4517. https://doi.org/10.1175/JCLI-D-12-00383.1

[71] Harrington, L. J., & Otto, F. E. L. (2020). Reconciling theory with the reality of African heatwaves. *Nature Climate Change, 10*(9), 796–798. https://doi.org/10.1038/s41558-020-0851-8

Sitography

- **USGS Earth Explorer**: United States Geological Survey.
  https://earthexplorer.usgs.gov
- **Copernicus Climate Data Store – ERA5**: ERA5 hourly data on single levels from 1940 to present.
  Copernicus Climate Data Store (CDS), ECMWF.
  https://cds.climate.copernicus.eu